A high throughput RNAi screen to identify modifiers of ALS8 aggregation using automated computational image analysis

A thesis submitted towards partial fulfillment of
BS MS Dual degree programme
by

Lokesh Pimpale
Department of Biology
Indian Institute of Science Education and Research, Pune

Thesis Advisor
Dr. Girish Ratnaparkhi,
Indian Institute of Science Education and Research, Pune

Certificate

This is to certify that this dissertation entitled "*A high throughput RNAi screen to identify modifiers of ALS8 aggregation using automated computational image analysis*" towards the partial fulfilment of the BS-MS dual degree programme at the Indian Institute of Science Education and Research, Pune represents original research carried out by Lokesh Pimpale, IISER Pune under my supervision during the academic year 2014-2015.

Girish Ratnaparkhi Date: 24th March 2015

Declaration

I hereby declare that the matter embodied in the report entitled "*A high throughput RNAi screen to identify modifiers of ALS8 aggregation using automated computational image analysis*" are the results of the investigations carried out by me at the at the Department of Biology, Indian Institute of Science Education and Research (IISER), Pune, under the supervision of Dr. Girish Ratnaparkhi, Biology, IISER, Pune and the same has not been submitted elsewhere for any other degree.

Lokesh Pimpale Date: 24th March 2015

Contributions

I declare that apart from myself and my project supervisor, the following people / facilities have contributed to different aspects of the research described in this thesis. These include:

1. Members of the NCBS-CCamp High Throughput screening facility. The Main Screen was conducted at the facility, as a paid service, initiated with inputs from Balaji Ramalingam. Assistance was provided for maintaining cell lines at NCBS and all imaging was carried out by Lokavya, Vandana and myself. I was present on-site, at Bangalore, when the screening methods were executed.
2. Synthesis of dsRNA. dsRNA for the 1200 genes screened were provided as a paid service by Chromous Biotech, Bangalore. dsRNA synthesis of ~80 genes was done in-house in IISER.
3. Image Analysis. Downstream Analysis of the 2.5 lakh images that were collected is still an ongoing process. The MATLAB program used to process and partially analyze the images was originally written by Balaji Ramalingam. The program has however been modified further, both by Balaji as well as by Dr. Kausik Chakraborthy, CSIR-IGIB, Delhi. Dr. Kausik's expertise in MATLAB programming and image analysis has been utilzed to explore different methdos of analyzing our data.
4. Lab members. Stable S2R+ plasmids for *pRM-VAP:GFP* and *pRM-VAPB^{P58S}:GFP*, were generated by D. Senthilkumar and data for Figure 10 was contributed by Kriti Chaplot.

Lokesh Pimpale

Acknowledgements

I would like to thank my project supervisor Dr. Girish Ratnaparkhi for constant guidance and support. Along with Girish, Senthil and Kriti have been involved with the project for which I am grateful. I would like to thank all the lab members of GR lab (Mithila, Bhagyashree, Vallari, Amar, Srija, Sindhuri, Ramya, Janavi, Apurv) for providing a work-suitable and encouraging environment. I would also like to thank Dr. Anuradha Ratnaparkhi, Dr. Richa Rikhy and RR lab members for their constant feedback and comments during lab meetings. I would also like to thank numerous other professors who have graded me and given important inputs regarding the project during semester poster sessions and presentations. I would like to thank Dr. Thomas Pucadyil for his constant feedback since the start of the project.

I would like to thank Balaji Ramalingam, Lokavya, Dhruv and Vandana at NCBS / C-Camp who have helped me plan my screen and its execution. The automated analysis would not have been possible without Balaji and Dr. Kausik Chakraborthy at IGIB. I would like to thank Dr. Madhusudhan for allowing me to use his computational workstation for image analysis. Imaging at IISER was assisted by Kriti and Vijay Vittal and thus I would like to thank them. I would also thank Dr. Nagaraj Balsubramanian and Dr. Sanjeev Galande for giving me access to EVOS microscopes.

I am grateful to my 2008 batchmates especially Sruthi, Bhargava and Hardik, members of academic committee at IISER, Dr. Sudarshan Ananth and my faculty advisor, Dr. Prasad Subramanian for supporting me during my 3rd year at IISER Pune. I would not have completed my BS MS without their support.

I would like to thank my parents who have been patient and have always given me independence to follow my interests. I would like to thank my sister and brother for supporting me at times of need. My maushi and kaka have been more than generous to accommodate me and provide me with numerous luxuries during my stay at Pune for which I am really grateful.

I would like to thank my friends at IISER Pune, NCBS and IGIB without whom working in the lab would not have been enjoyable. At last I would like to thank Raunaq and Kriti, who have been responsible for keeping me sane through all the ups and downs during the project and PhD applications.

Index

Abstract

Protein aggregation is a hallmark feature of human neurodegenerative diseases (NDs). In familial NDs the affected genetic locus is perturbed by point / missense mutation that codes for a protein which misfolds and forms intracellular inclusions. Large-scale whole genome RNAi screens using cells in culture are useful to identify proteins/genes that may modulate (enhance or suppress) the formation of cellular inclusions in disease conditions. These modulators could help us understand relationship between aggregation and neuronal cell death.

For my thesis work, I present the standardization and validation of a *Drosophila* S2 cell based high-throughput screen for identifying genes that can modulate the aggregation of the ALS8 locus *VAP*. We have established stable S2 cells expressing inducible VAPB^{P58S}:GFP and VAP:GFP fusions that can be monitored for aggregate formation over time, by epifluorescence microscopy. Using high-throughput gene knockdown and automated imaging, we have collected data for the effect of knockdown of 1200 independent genes on VAPB^{P58S}:GFP aggregation. The imaged data has been analyzed using a custom MATLAB program and a list of modifiers has been generated. One key result is that modifiers include other ALS loci such as *ALS1/SOD1*, *ALS2/Alsin* and *ALS10/TDP43*.

As a final step of my study, I have characterized and validated the interaction of *ALS1/SOD1* with VAPB^{P58S}. My investigations suggest that different ALS loci can interact with VAPB^{P58S} and their levels can affect the propensity / degree of protein aggregation. This finding has major implications as it may lead to a better mechanistic understanding of onset and progression of motor neuron disease.

List of Figures & Tables

Introduction

Amyotrophic lateral sclerosis also called “Lou Gehrig’s disease” (Cleveland and Rothstein, 2001; Tarasiuk et al., 2012) is a progressive, fatal neurodegenerative disease characterized by loss of motor neurons. This leads to gradual paralysis and death of the patient within 2-5 years post diagnosis. Most often, the disease occurs sporadically; the patients lack any familial history of the disease. In 5-10% of the patients, the disease occurs due to inheritance of dominant mutation . Many associated genetic loci have been discovered, with the first locus ALS1/SOD1 discovered in 1993 (Rosen et al., 1993). Since then, over a dozen independent genetic loci **(Figure 1)** (Pasinelli and Brown, 2006) in humans have been associated with ALS and a large volume of research has been done to understand relationships between these genes and cellular dysfunction (Robberecht and Philips, 2013). While these studies have demonstrated the wide-range of consequences of the mutant protein on cellular function, no clear unifying mechanism has emerged that might explain the selective death of motor neurons (Andersen and Al-Chalabi, 2011; Mulligan and Chakrabartty, 2013; Turner et al., 2013; Walker and Atkin, 2011).

One common feature of ALS and other neurodegenerative disease is the aggregation of mutant proteins (Chhangani and Mishra, 2013). These aggregates are thought to be a byproduct of protein misfolding, which recruits or entangles other proteins in the cytoplasmic inclusion. The cell has pathways that deal with and regulate misfolded aggregates. These include the Unfolded protein response (UPR), proteasome / ubiquitin system and autophagy (Chhangani and Mishra, 2013; Mulligan and Chakrabartty, 2013). For reasons not completely understood, the presence of mutant protein in aggregates is strongly linked to neuronal cell death. Since ALS has a large sporadic component and the familial loci are diverse, with no obvious relationship with each other, it has been suggested (Cluskey and Ramsden, 2001) that the etiology of the disease is multifactorial with the onset and progression dependent on a complex interplay between genetic factors, stress, glutamatergic excitotoxicity, organelle homeostasis and the cellular response to chronic aggregation of proteins (**Figure 1A**) (Chhangani and Mishra, 2013; Robberecht and Philips, 2013).

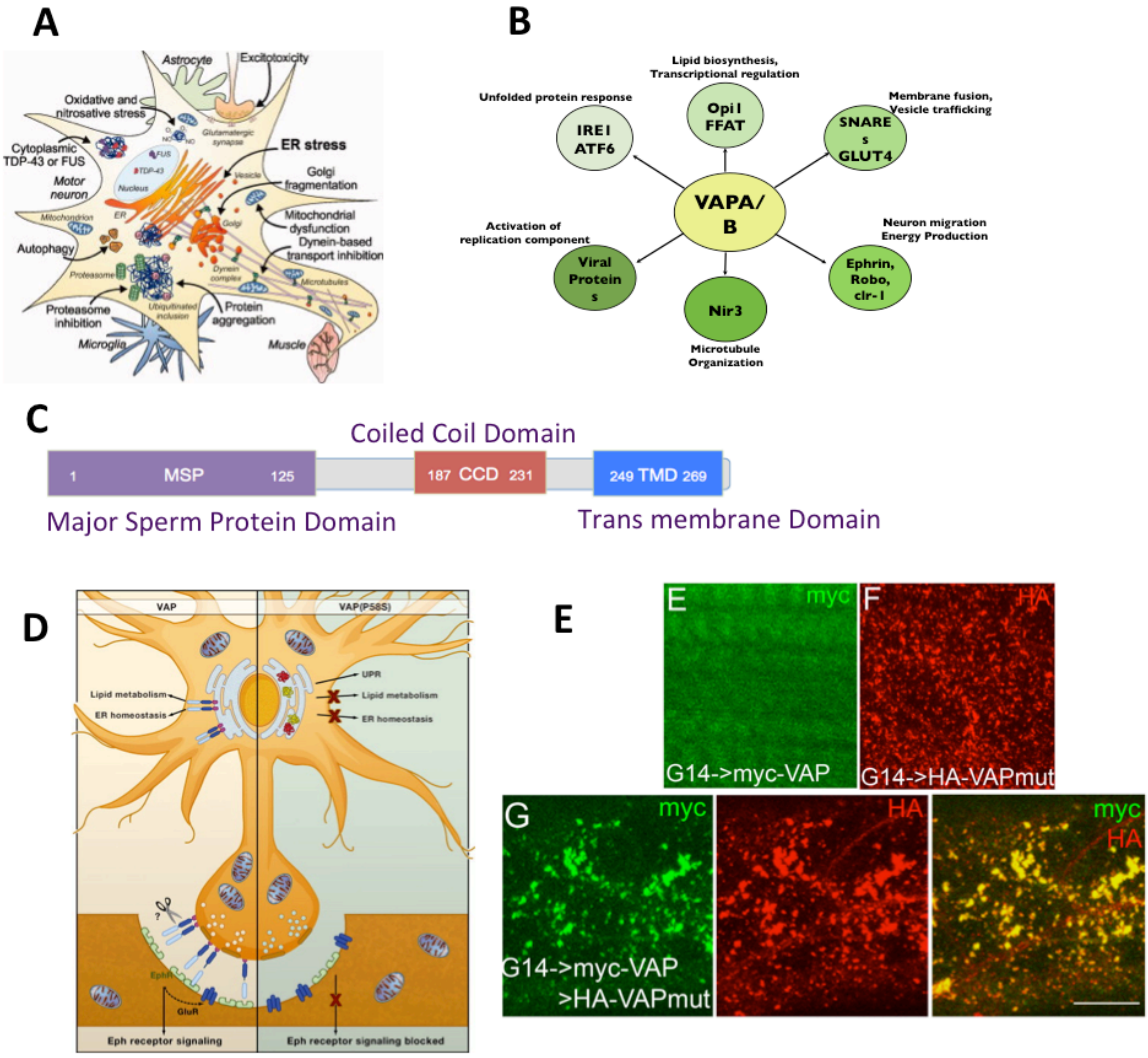

Figure 1: ALS; Many Loci, complex multifactorial etiology

A. Genetic loci governing many different processes selectively affect motor neurons, which are influenced by surrounding cells, such as presynaptic neurons, astrocytes and microglia, in disease. These processes include: induction of ER stress; aggregation of misfolded proteins and formation of intracellular inclusions; macroautophagy; oxidative and nitrosative stress; excitotoxicity mediated by over-stimulation of postsynaptic glutamate receptors; redistribution of TDP-43 and FUS from the nucleus to the cytoplasm; fragmentation of the Golgi apparatus; dysfunction of mitochondria and activation of mitochondrial apoptotic pathways; inhibition of microtubule-based dynein-mediated intracellular and axonal transport, and; inhibition of the ubiquitin-proteasome system (Adapted from(Walker and Atkin, 2011).

B. VAP/ALS8 is one genetic locus that is linked to ALS. VAP is associated with the ER and has been shown to affect diverse cellular functions. A missense P56S mutation in VAP causes ALS in humans.

C. VAP contains a N-terminal major sperm protein (MSP) domain which is cleaved and acts as a secreted ligand for ephrin receptors, a coiled coil domain (CCD) involved in inter and intra-molecular interactions with VAP and SNARE's and a single pass trans-membrane that anchors the protein to its primary location, the ER membrane.

D. Lipid metabolism, ER homestasis and Eph signaling are amongst the cellular events that are perturbed in response to the VAP^{P58S} mutation (Tsuda et al., 2008) in flies.

E. VAP^{P58S} protein forms intracellular aggregates. These cellular inclusions, amongst other proteins, contain VAP and ubquitin (Adapted from Ratnaparkhi et. al., 2008).

In 2004, Mayana Zatz and collegues (Nishimura et al., 2004) identified and mapped a new locus (ALS8) for ALS in a large white Brazilian family (Nishimura et al., 2004). The novel missense mutation P56S (P58S, in *Drosophila*) was found to be in the vesicle associated membrane protein (VAMP) / synaptobrevin associated protein B (VAPB; hereafter referred to as VAP)(Lev et al., 2008). In *Drosophila*, *dVAPB*, the fly ortholog, has been shown to regulate bouton size and microtubule organization at the neuromuscular junction (Pennetta et al., 2002). *Drosophila* has long been used to study neurodegenerative diseases due to a well-studied nervous system and the availability excellent tools for manipulation of genes (Bier, 2005; Zhang et al., 2010). *Drosophila* models of ALS8 generated show that VAP^{P58S} aggregates and recruits wildtype protein to these aggregates eliciting a dominant negative effect (Chai et al., 2008; Ratnaparkhi et al., 2008; Tsuda et al., 2008). In these models, some features of the human disease, especially the aggregation of the mutant protein is recapitulated when mutant human or dVAPB is expressed in neurons or muscles (Ratnaparkhi et al., 2008).

In addition to animal models (Chiu et al., 1995; Gurney et al., 1994; Murakami et al., 2012; Turner and Talbot, 2008; Vaccaro et al., 2012), cell based models, using cells in culture for exploration of disease onset and progression, are popular (Chiu et al., 1995; Gkogkas et al., 2008; Pennetta et al., 2002; Teuling et al., 2007; Tsuda et al., 2008). This popularity stems from their ease of use and faster data collection. A major advantage of cell models is that they are amenable to high throughput assays. *Drosophila* S2 cells are amongst the most extensively used for high throughput RNA interference assays because of their ease of maintanence, low cost for growth and high efficiency knockdown of transcripts using RNA interference (Zhang et al., 2010).

In our study, we have generated a new system for efficient screening of modifiers of VAP aggregation by high throughput screening and automated computational image analysis (**Figure 2**). The components of the system are as follows. First we have developed inducible *Drosophila* S2R+ cell lines that allow fast and accurate measurement of VAP:GFP and VAP^{P58S}:GFP aggregation. Second, we have standardized conditions for measuring kinetics of aggregation,

using fluorescent imaging, in a 384 well format. Third, we have developed methods to analyze the images gathered and finally we have generated a list of genes, which on knockdown significantly affect the kinetics of VAP^{P58S}:GFP aggregation. A single gene from our modifier list has been chosen for validation and its effect on VAP^{P58S} aggregation was confirmed both in S2R+ cells and *Drosophila* third instar larval brain.

Goals

(i) Develop a Schneider cell system for VAP^{P58S} that is suitable for a genome wide dsRNAi screen.
(ii) Generate a list of modifiers of aggregation through the dsRNAi screen combined with high throughput imaging and automated analysis.
(iii) Validate a subset of discovered hits to gain insight into the mechanism of neuroaggregation.

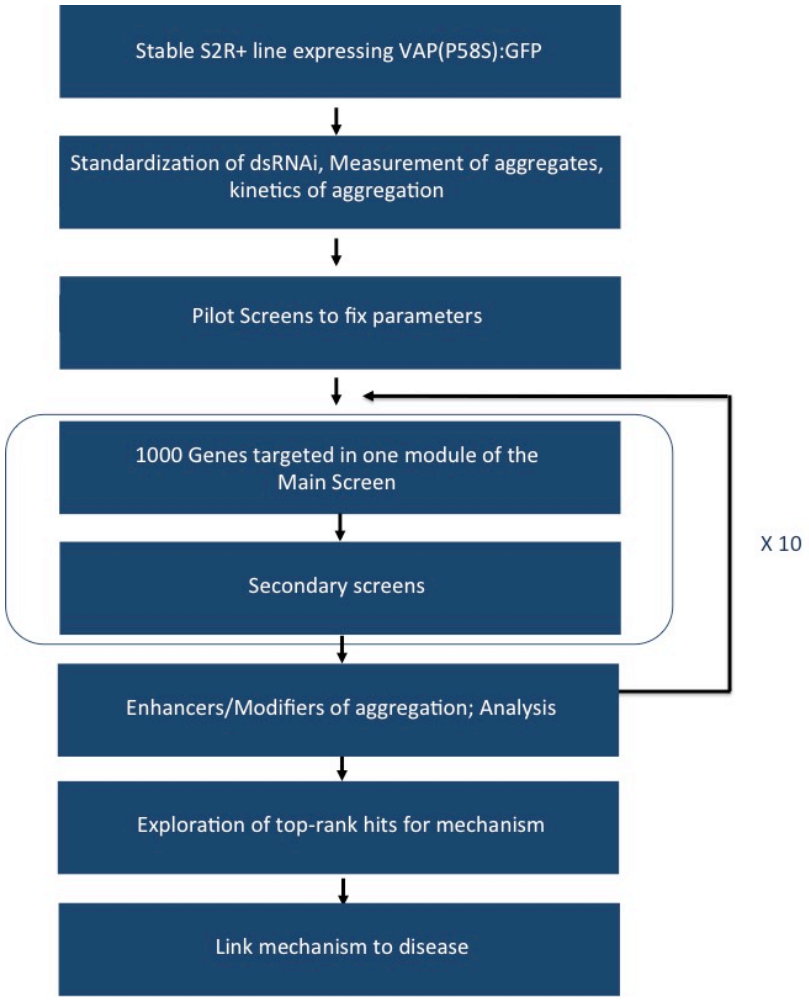

Figure 2: A Schneider cell aggegation system to identify genetic modifiers of VAP^{P58S}aggregation. A flow chart for developing an aggregation screen. Critical standardization steps including development of cell lines lead to a pilot screen to fix parameters and finally to the main screen using an automated imaging system. We plan to screen one thousand genes per module. Information on valid modifiers will be used to chose the next 1000 genes in the screen. Finally, the list of modifiers will be used to understand mechanistic basis of regulating aggregate formation and this might lead to a better understanding of initiation/progression of ALS.

Materials and Methods

Handling of Schneider cells: *Drosophila* S2R+ cells were procured from the laboratory of Dr. Satyajit Mayor, NCBS. The cells were maintained in Schneider cell Media (#21720-024; GIBCO) with 10% Heat inactivated Fetal Bovine Serum (FBS, #10270; GIBCO). Batches of cells were frozen in 10% DMSO (D2650; Sigma) and stored in liquid nitrogen following DRSC protocol (http://www.flyrnai.org/DRSC-PRC.html).In general, after reviving, cells were discarded after 25-30 passages. Cell were maintained at 23° C, and split every 4 days at a ratio of 1:5.

Generation of Stable cell lines: *VAP* and VAP^{P58S} cDNA sequences were cloned into *pRM*-GFP plasmid at the BamH1 restriction site in the MCS. The *pRM* vector is a vector with an inducible metallothionein promoter that is sensitive to concentrations of CuSO4. *pRM-VAP:GFP* and $pRM\text{-}VAP^{P58S}\text{:}GFP$ plasmid were co-transfected with *pCo-Hygro* in S2R+ cells using Effectene Transfection Reagent (301425; QUIAGEN). The ratio of *pRM*: *pCo-Hygro* was 15:1. Hygromycin B was obtained from Invitrogen (10687-010). Cells were selected in 0.2 mg/ml Hygromycin for 10 passages and samples intermittently checked for GFP expression post $CuSO_4$ induction. A *pRM-GFP* stable line was made in a similar fashion using Mirus (TransIT 2020; MIR 5400) reagent with ratio of *pRM*: *pCo-Hygro* of 10:1.

dsRNA preparation: dsRNA for the high throughput screen was generated by Chromous Biotech, Bangalore and plated into 384 well plates in preparation for the experiment. The library used as a template for generating dsRNAs was procured from Open Biosystems (RDM1189 and RDM4220). dsRNA for all primary experiments, the pilot and the validation screens was generated in-house at IISER using GOLD collection (DGRC, Indiana; https://dgrc.cgb.indiana.edu/vectors/Gold) and AMBION Megashortscript kit (AM1354) using standard protocols. (http://tools.lifetechnologies.com/content/sfs/manuals/cms_055515.pdf). cDNA templates used were individual clones from the BDGP Gold collection.

Reviving clones from the GOLD cDNA collection: The GOLD cDNA collection contains sequenced and verified clones of *Drosophila* genes. The collection consists of ~ 7000 Glycerol stabs of bacteria, each with a unique gene. Copies of these stocks are stored at IISER at -80°C.

Image acquisition and data analysis: Imaging for the pilot screen was done using in-house OLYMPUS IX81 system using MT20 florescence. Objective used was 20X S-Apo objective with Hamamatsu OrcaR2 CCD camera. Images were captured from Xcellence RT software. Images were acquired in 2 binning, 672x512. Imaging for the high throughput screen was performed byTHERMO Array Scan VTI HCS system. Dual- channel images from ten fields in each well were captured using a 20X air objective and an EMCCD camera. The FITC channel was used for checking the level of GFP expression and the DAPI channel for cell nuclei. Images from the FITC and DAPI channels in each site were quantified using MATLAB code to calculate the parameters of aggregated population of cells and determine the cell number within each field. To ensure accuracy, manual counting was performed on handpicked wells on the plate and the results were comparable to those obtained from automated analysis. Numbers of cells present in each field were calculated from the images taken from DAPI channel. Approximately 4000 cells were scanned for each well and 12000 for each dsRNA knockdown.

Targets obtained from the screen were validated after imaging on EVOS FL Auto Cell Imaging system. All the imaging was done on 20x air objective unless mentioned otherwise. FITC, DAPI and DIC channels were used to image GFP-tagged aggregates, cellular nuclei and cells in each field, respectively. Counting was performed manually and auto-count feature using software package provided with the microscope.

Plasmids:Clones streaked from GOLD collection were grown overnight. Secondary incubation was done in 5ml Luria Broth for 12 hours. Cells were pelleted down and processed using QIAGEN Miniprep kit (27104; QUIAGEN). (https://www.qiagen.com/in/products/catalog/sample-technologies/dna-sample-technologies/plasmid-dna/qiagen-plasmid-kits/)

Primers:Desiging of primers was done using NEXTRNAi (http://www.nextrnai.org/). T7 promoters were incorporated at 5' end of the primer for *in vitro* transcription reaction. siRNA length for specificity used were 16 nucleotides with amplicon size of 150-250 base pairs.

Western Blotting: S2R+ cells / Stable cell lines were centrifuged at 3000 rpm in an Eppendorf 5414R and the cell pellet was processed with 2X SDS Dye at 95°C and re-centrifuged at 10000 rpm for 10 minutes. Cell extracts were separated on 10% SDS-PAGE and transferred onto 0.45 mm PVDF membrane (Millipore). Membranes were blocked for 1 hour in 5% skimmed milk in TBS-0.1% Tween-20 at room temperature and probed with 1:10,000 diluted anti-Tubulin (3H3085; Santa Cruz Biotechnology), 1:20,000 diluted anti-VAP (custom antibody generated in the lab), 1:10,000 diluted anti-GAPDH (AB8245; AbCam), 1:10,000 diluted anti-GFP (A6455; Invitrogen) or 1:1000 diluted anti-HA (04902; Millipore). Anti-rabbit and anti-mouse secondary antibodies conjugated to horseradish peroxide (Pierce) were used. Blots were developed with Immobilon Chemiluminescent Substrate (LuminataClassico Western HRP substrate from Millipore) using a LAS400 Fuji imaging System. Quantitation was performed after normalization with tubulin/GAPDH and plotted with error bars representing standard deviation ()

Fly strains : Fly lines were maintained at 18°C on standard corn meal agar medium. UAS-GAL4 system was used for overexpression of transgenes. UAS-VAP wildtype and VAP^{P58S} lines used for fly experiments have been described in Ratnaparkhi et al 2008. Canton S flies were used as wildtype control flies. Trip lines from SOD1 (34616), TBPH (29517) and VAP (27312) knockdown were obtained from Bloomington stock centre.

Immunostaining : Five brains were dissected from 3rd instar larvae and processed for immunostaining assay. 0.1% Triton-X with 4% paraformaldehyde was used for fixation followed by washes with PBS. Blocking treatment and washes were performed with 0.3% Triton-X with 2% BSA. Brains were stained with 1:500 diluted Anti-VAP antibody (custom antibody generated in the lab) and 1:1000 anti-rabbit secondary was used. Five brains for each sample were imaged under 60X oil objective of Ziess LSM 710 Confocal Microscope.

Results

1. Development of cell lines suitable for high-throughput screening

S2R+ cells have been extensively used for high throughput screening. The popularity of S2 cells is based on their ease of use, effective knockdown of specific mRNA and flat morphology for microscopy (Zhang et al., 2010) (D'Ambrosio and Vale, 2010). In order to screen for modifiers of VAP^{P58S}aggregation, we chose to fuse a fluorescent GFP to VAP so as to visualize the aggregates by epifluorescence. This would allow us to visualize and image aggregates without resorting to downstream antibody staining. The GFP fusion would also allow us to measure live, the kinetics of aggregation by measuring the increase in aggregates with increased protein accumulation in the cell as a function of time.

Proteins are usually tagged at the N or C terminus with GFP. Tagging proteins with GFP may perturb folding as well as localization and thereby protein function within the cell (Stadler et al., 2013). An important step in the setting up of the screen was to characterize the different possible GFP fusion variants and confirm that, as seen in the untagged scenario, the mutant versions aggregate while the wild-type versions do not. The variant most suitable for the screen would be chosen for further studies. We cloned (See Methods section) and tagged both VAP & VAP^{P58S} at both N and C terminal with GFP (**Figure 3**). The fusion proteins could be expressed in cells by adding $CuSO_4$ to the medium, which would drive transcription via the metallothionein promoter.

pRM-VAP:GFP, pRM-VAP^{P58S}:GFP, pRM-GFP:VAP & pRM-GFP:VAP^{P58S} plasmids were transiently transfected into S2R+ cells. Twenty-four hours post transfection; 500 µM CuSO4 was added to the medium in order to induce VAP protein expression. The numbers of cells with aggregates were visualized over time at 16, 24, 36 and 48 hours by fixation with 4% paraformaldehyde, incubation with DAPI and dual channel imaging under DAPI and GFP channel. In each case, the number of cells in a field was counted (DAPI positive cells), as well as the

total number of cells with aggregates.

The GFP:VAP^{P58S} protein aggregated as expected, but the control, GFP:VAP fusion had a strong tendency to aggregate as early as 24 hours. In contrast, the VAP:GFP fusion did not aggregate significantly, with only a small number of cells with aggregates seen after 48 Hours. The VAP^{P58S}:GFP expression showed strong aggregation, in contrast to the wild type. Based on the above results, where the C-terminally tagged lines showed the strongest contrast between wild-type and mutant, we decided proceed with the C-terminally tagged pair (VAP:GFP and VAP^{P58S}:GFP) for further experiments.

As we planned to use the cell lines extensively for future experiments, we decided to generate stable cell lines for all 5 constructs (*VAP:GFP, VAP^{P58S}:GFP, GFP:VAP, GFP: VAP^{P58S} & GFP*). The stable cell lines would allow us to avoid the variability in transient transfection with each experiment and these lines could be stored in liquid nitrogen for replicate experiments. Independent stable cell lines were made for the five constructs and characterized. The 'aggregation' phenotype and kinetics of the stable cell lines was similar to that of the transiently transfected ones. One problem we faced with stable lines was a decrease in the percentage of cells expressing aggregates as compared to the transient-transfected counterparts after multiple passages during the process of stable cell formation. In general, with transient transfection we saw 50-70% cells transfected (GFP positive cells), while at the end of the stabilization process, the number of cells expressing GFP dropped to 10%. A solution was found by clonal expansion of the C-terminally tagged GFP fusion lines, which show approximately 25% cells expressing aggregates in each field upon induction with 500uM of $CuSO_4$ for 24 hours. Also, the generated stable cell lines were continuously maintained under hygromycin selection to maintain the percentage cells expressing protein of interest.

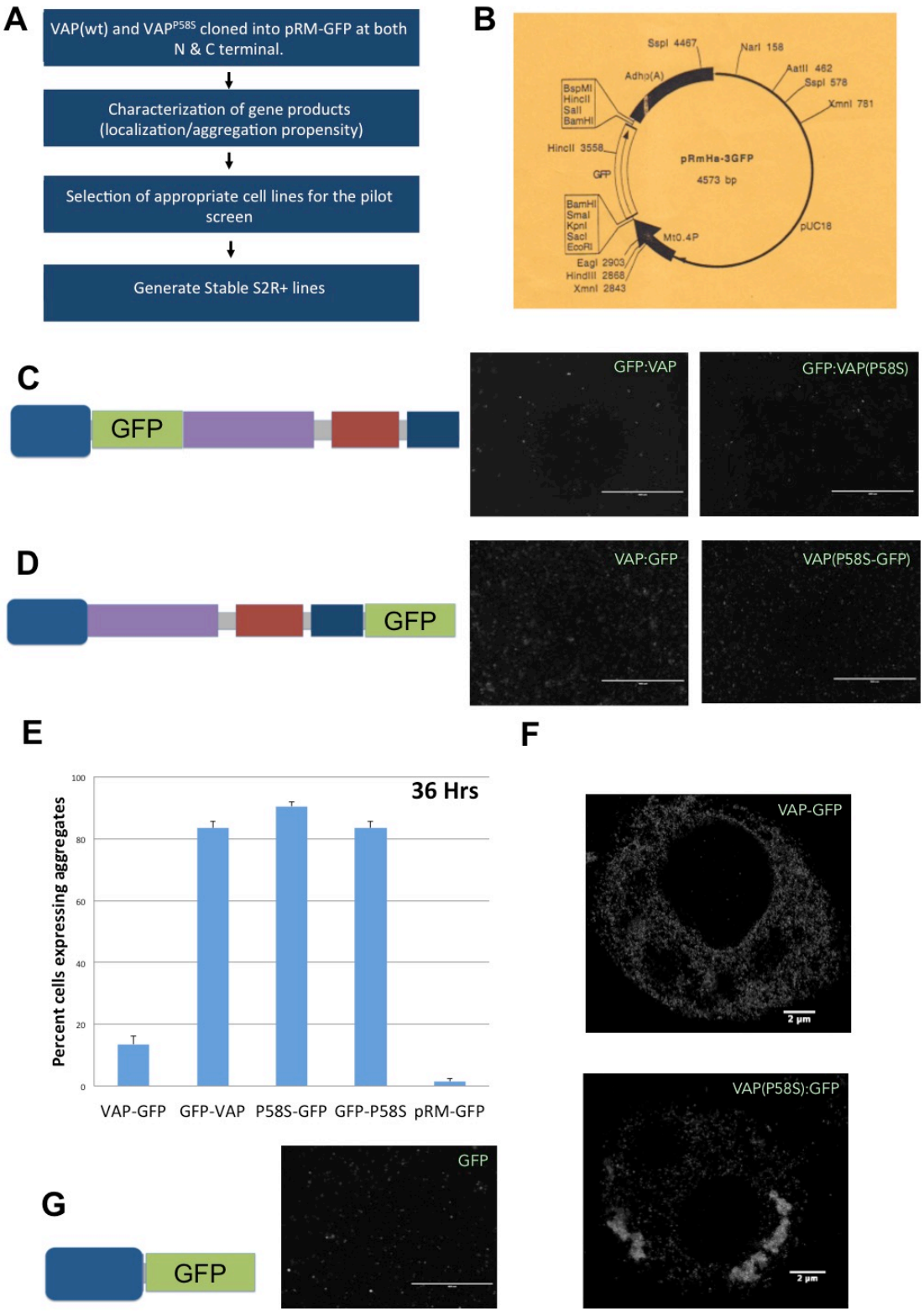

Figure 3: Develop stable cell lines suitable for high throughput screening.

A. Flowchart for generation and selection of appropriate GFP tagged constructs for screening.

B. pRM-GFP was used to clone *VAP* and *VAP^{P58S}*.
C. VAP and VAP^{P58S} were expressed with N-terminal GFP fusions.
D. VAP and VAP^{P58S} were expressed with C-terminal GFP fusions.
E. Percentage cells expressing aggregates in GFP positive cells in each case were scored 36 hours post induction with 500μM $CuSO_4$. The C-terminal fusions behaved as expected with strong aggregation seen in the mutant but not in wild type. The N-terminal GFP fusions for VAP however showed aggregates for both wild-type and mutant. Error bars indicate SD. (GFP positive cells counted for each transfection = 200)
F. A high resolution image showing inclusions in cells expressing VAPB^{P58S}:GFP and their absence in VAP:GFP. (L) C-terminal GFP tagging of wild type and mutant VAP protein. The images were collected using Super resolution (Ground State Depletion) microscopy.
G. A Stable line expressing GFP was used as a control for downstream experiments. Stable lines were also made for VAP:GFP, VAP^{P58S}:GFP, GFP:VAP and VAP^{P58S}:GFP.

To identify modifiers or regulators of aggregation from our planned screen, we wanted to select a robust parameter that could be reproducible and would be sensitive to our assay. In order to choose a parameter we artifically expressed increasing concentrations of VAP-GFP or VAP^{P58S}:GFP protein in stable cell lines by inducing the metallothionin promoter with different concentration of $CuSO_4$(0 μM, 250 μM, 500 μM, 750 μM & 1000 μM). After image acquistion, we attempted to quantify various parameters like number of cells expressing aggregates, number of aggregates per cell and size of aggregates as a function of increasing concentration of $CuSO_4$. Using either manual counting or programs available as part of the microscope suite or by custom MATLAB programs (described in Image Analysis section), we could efficiently and robustly count the percent of cells that showed aggregation.We could not effectively count number or intensity of individual aggregates due to the low resolution of the 20X objective; a higher objective decreased the number of cells per field and increased collection time significantly. Importantly, the percent cells expressing aggregates increased linearly with increasing amount of $CuSO_4$ and also increased with time; 24 to 48 hours (**Figure 4**).This parameter (percent cells with aggregates / total number of cells) was, thus, chosen as a simple but robust parameter for high throughput screening that was sensitive to protein levels of VAP^{P58S} inside the cells. As part of the characterization of the cell lines, we showed that knockdown of *VAP* or *GFP* by RNA interference led to a dramatic decrease in the percent cells with aggregates, indicating that one could modulate the formation of cellular aggregates by modifying expression of protein levels.

2. Standardization of screening and parameters for high-throughput screening

The VAP^{P58S}:GFP was the primary line used for the high-throughput screening. The VAP:GFP and GFP stable lines were used for downstream validation of modifiers that were identified in the primary screen. As a preliminary to the high-throughput screen we used a pilot screen in-house to standardize parameters for the high throughput screen. Again, we used a concentration dependent kinetic experiment to validate increase of percent cells with VAP^{P58S}:GFP aggregates in a 96 well Corning Glass bottom plate. Time points measured were 24, 36 & 48 hours for 0 µM, 250 µM, 500 µM, 750 µM and1000 µM $CuSO_4$. VAP or GFP Knockdowns were performed by incubating cells with dsRNA added Serum free media for about 30 minutes, followed by addition of serum complete media. The 48-hour time point was discarded after this exercise as a there was a considerable increase in population of floating cells at 48-hour time point, interfering with the focusing of the microscope. Live cell imaging was also discontinued post the pilot screen as it was seen that there was high background auto fluorescence in live cells due to presence of media in wells. Also, without fixation, DAPI staining of live cells was not robust. Since cells are confluent at the 48-hour time-point, using watershed algorithm to segment cells using DIC images was highly inaccurate. Thus, to mark cells in a better and accurately quantifiable method we fixed cells / stained nuclei with DAPI and imaged using 20x air objective for time points at or less than 36 hours.

For the pilot screen, the percent cells showing aggregates for standard curve for the pilot run were counted manually and by using the imaging software available in the microscope (EVOS FL microscope).

We also started the process of developing a MATLAB code for automated image analysis using the images generated in our pilot screen. As described in later sections images collected by automated imaging were quantified in a high throughput manner using a custom MATLAB code.

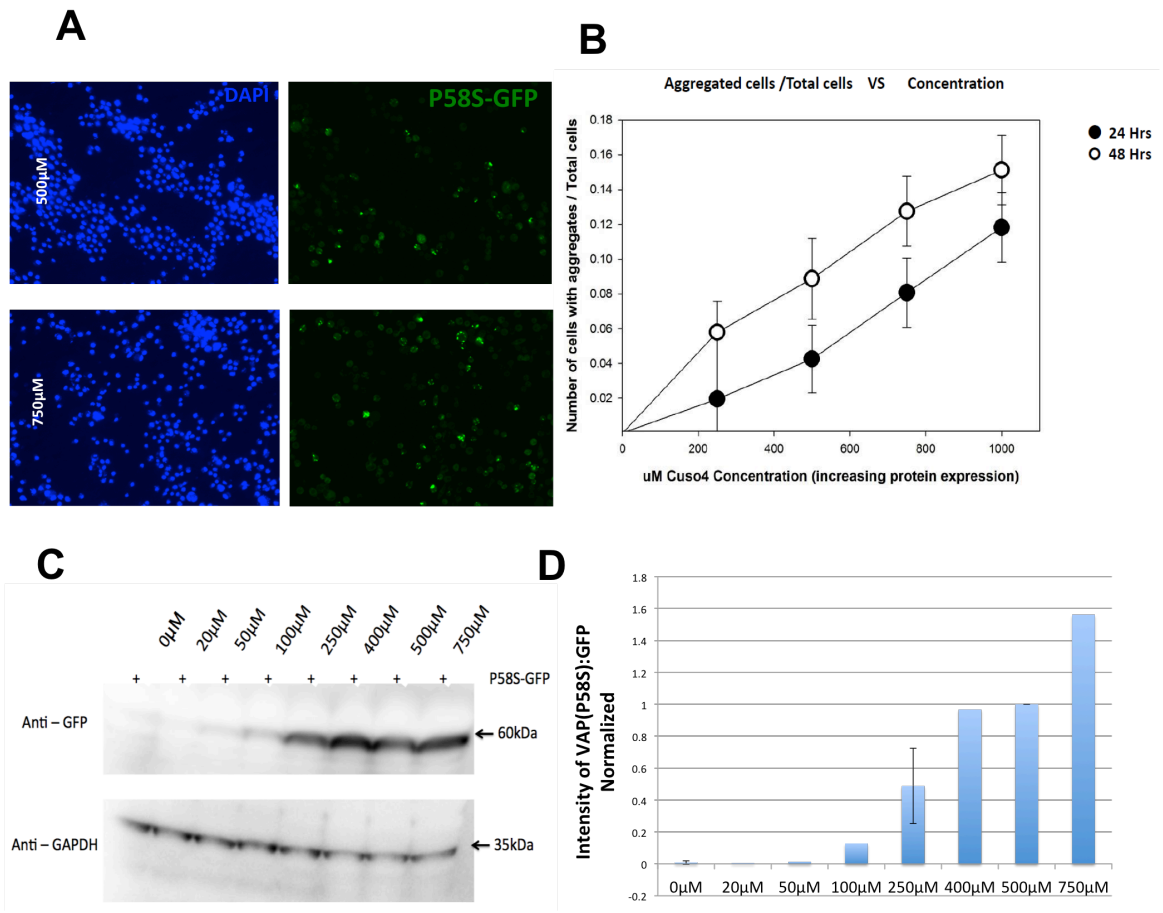

Figure 4: Standardization of screening parameters.

A. Images of VAP^{P58S}:GFP induced with 500uM and 750uM $CuSO_4$ and visualized in GFP and DAPI channels. DAPI staining was used to count total cells while the GFP channel marked cells expressing VAP^{P58S}:GFP.
B. Concentration dependent increase of percent cells (GFP/Total X 100) showing GFP aggregates with increasing $CuSO_4$ (0 µM, 250 µM, 500 µM, 750 µM and 1000 µM). Cells with aggregates also increased with time (24 hours vs. 48 hours). The percent GFP positive cells was a simple, quantifiable robust parameter that was reproducible across systems and over biological replicates.
C.VAP^{P58S}:GFP protein levels also increase with increasing concentration of $CuSO_4$, as measured by Western blotting using the anti-GFP antibody.
D. Quantification of 60kDa VAP^{P58S}:GFP band observed in westerns probed with Anti-GFP. Intensity was measured and quantified using ImageJ and normalized with respect to un-induced control (0uM). Error bars represent SD. (N=2)

Pilot screens were conducted at IISER (**Figure 5A**) to fix the concentration of dsRNA, hours for knockdown, optimal concentration of $CuSO_4$ for expression of protein, time points for image collection and to test expression of stable lines generated (VAP:GFP & VAP^{P58S}:GFP). These pilot screens were usually executed with all three stable lines, VAP^{P58S}:GFP, VAP:GFP and GFP. dsRNA

was used to knockdown both *VAP* and *GFP* to reduce expression / aggregation of VAP:GFP and VAP^{P58S}:GFP.

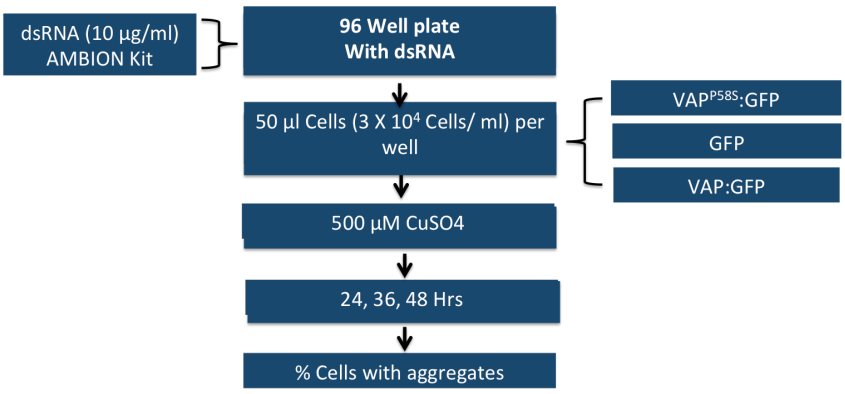

B

FAMILY OF GENES
VAP interactors & genetic network (400)
Peptidyl-proryl isomerases (28)
mTOR pathway (22)
ALS loci (56)
Unfolded protein response (61)
FFAT proteins (47)
Lipid Biosynthesis (106)
Ubiquitin & ligases (153)
Ubiquitin – proteosome (98)
SUMO (8)
Autophagy (117)
Chaperones (95)
Mitochondrial proteins (3)
nFkB pathway (106)

C

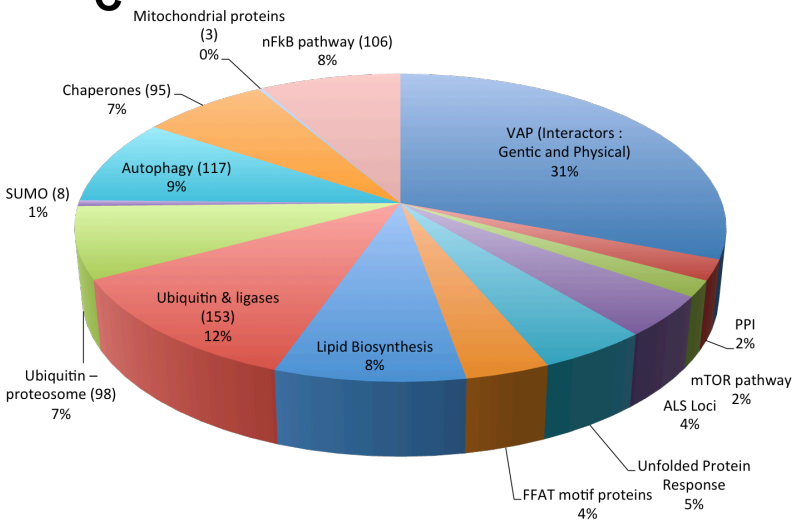

Figure 5: Pilot screens and choice of targets

A. Pilot screens in 96 well glass bottom plates were performed to fix critical parameters for the main screen. Three time points, 24, 36 & 48 hrs post induction by CuSO4 were used to collect images on Olympus IX81 microscope. dsRNA concentrations were fixed (10 ug/ml) and dsRNA was added 48 hours before induction. At each time point, cells were fixed, stained with DAPI and washed with PBS. 5 images were collected per well by manual focusing at a magnification of 20X. dsRNA knockdown of VAP or GFP lead to effective knockdown of VAP^{P58S} aggregation.

B. Choice of genes for the first high throughput set based on modifiers discovered in an earlier VAP screen (Deivasigamani et al., 2014). 1200 genes were tested and they could be divided into 14 independent categories.

C. Gene Ontology representation of the 1200 genes chosen for the first set of high throughput screening. Future sets (n X 1000) will be based on results of the first set.

Previous genome-wide screens performed using cell-based approaches (D'Ambrosio and Vale, 2010; Zhang et al., 2010) have shown the difficultly posed with identification of 'true' hits, which directly modify a phenotype, from 'false' hits which act in an indirect manner by having a global effect on cellular machinery to change the phenotype being scored. We, thus, chose to perform a screen targeted to specific family of proteins rather than targeting the whole genome. Primarily, this included the previously identified genetic interactors for wild type VAP protein in the lab (Deivasigamani et al., 2014) and various other known ALS loci ((Renton et al., 2014); (Abel et al., 2012; Andersen and Al-Chalabi, 2011). Other categories included genes pertaining to ALS like Ubiquitin, Ubiquitin-Proteosomal pathway genes, autophagy etc. The list of genes screened and their Gene Ontology (GO) distribution can be seen in **Figure 5B**.

3. The high-throughput screen

The final screen was performed at screening facility at CCAMP-NCBS, Bangalore. Parameters standardized for the 96 well-plate formats were modified to suit the 384-well/high-throughput format (**Figure 6**). A flowchart of the steps followed is displayed (Figure 6A). The time points chosen for visualization of aggregates were 24 & 36 hours post $CuSO_4$ induction with 500 µM $CuSO_4$ for used for induction.50 µl of cells (3 X 10^6 / ml) were plated in each well for the 384 well plate obtained from Porvair. Each target dsRNA knockdown experiment was run in triplicate. **Figure 6B** lists the parameters used for the final screen.

To account for systemic errors like well errors or plate-errors that can arise due to errors in sizes of wells leading to inaccurate data collection; we randomized the position of each of the triplicate data (**Figure 6D**).

A

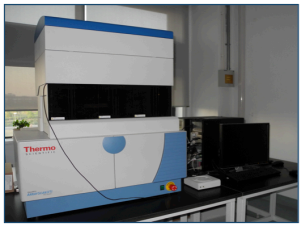

Chromus dsRNA (10ug/ul)

384 well plates spotted with dsRNA (16 plates)

50 µL cells spotted per well for 48 hours

Stable line VAP (P58S-GFP)

500µM CuSO4 induction post knockdown for 24 and 36 hours

20 images per field using THERMO Cellomics Array Scan VTI.
20x – GFP and DAPI channel

1200 genes

MATLAB analysis

Percent cells expressing aggregates

Mean GFP levels

List Enhancers/Suppressors

B

10ug/ml dsRNA concentration for 48 hours

500µM $CuSO_4$ induction

24 & 36 hour Time point in triplicates

→

Primary screen
VAP^{P58S}-GFP

Secondary screen
PRM-GFP / VAP-GFP/
GFP-VAP^{P58S}

↓

384 well Corning, flat bottom plates

20 fields per well

Fixing – Washing x2 – DAPI – Washing x2 – Imaging

←

THERMO Cellomics array scan Vti

Custom MATLAB Script for image analysis

C

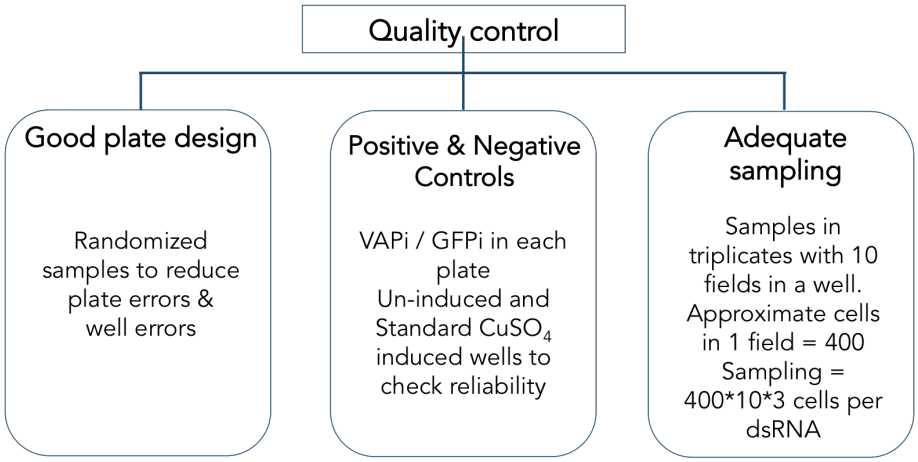

D

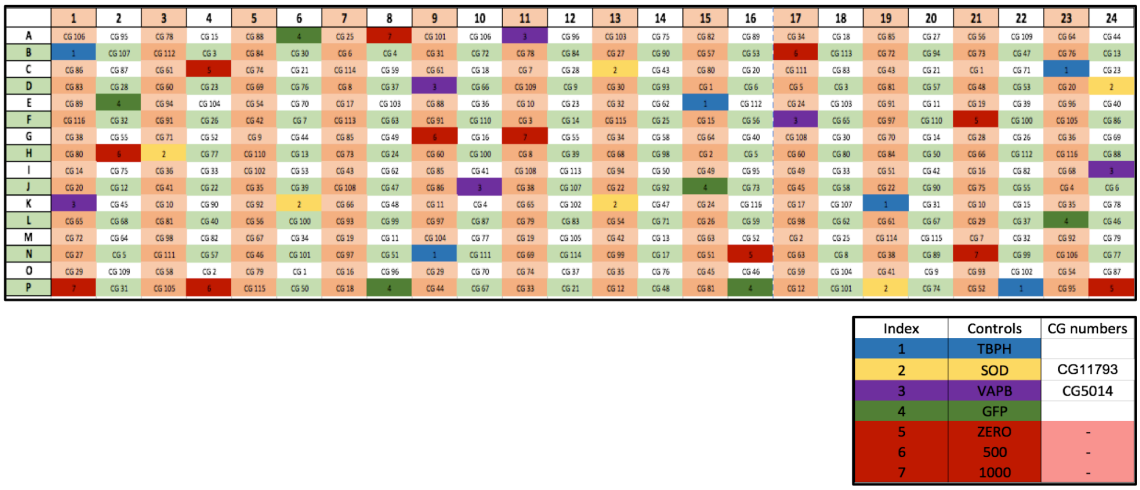

Index	Controls	CG numbers
1	TBPH	
2	SOD	CG11793
3	VAPB	CG5014
4	GFP	
5	ZERO	-
6	500	-
7	1000	-

Figure 6: A high througput screen based on parameters established in pilot screens.

A. Workflow of the steps executed for the high throughput screen. The screen was conducted on a 16 X 384 well Porvair glass bottom plate(s) using a THERMO Cellomics Array Scan VTi. dsRNA for 1200 unique genes was procured from Chromous Biotech.

B.Standardized parameters for the final screen. Concentration of dsRNA, duration for knockdown and optimal concentration of inducer that could allow monitoring of percent cells expressing aggregates increasing or decreasing were fixed as mentioned. The primary screen was performed on VAP^{P58S}-GFP cell line in 384 well plates with glass bottom. For imaging, an automated microscopy platform from THERMO was used.

C. Controls included in each plate to ensure the proper functioning of stable cell line and knockdowns carried out by dsRNAs. Each gene was screened in triplicates and these were randomly plated in the 384 well plate to reduce well and plate errors. Multiple positive and negative controls were included in each plate to ensure dsRNA treatment. Around 12000 cells were screened and imaged for each target knockdown.

D. Template for a sample plate shown (Plate map). Each plate contained 7 controls occupying 42 wells. 114 unique genes were screened in each plate. Few genes were kept as overlap between multiple plates to check for their consistency and reproducibility.

Each plate contained multiple controls that ensured the quality control for each plate (**Figure 6C, D**). First, non-dsRNA treated $CuSO_4$ controls induced with different concentrations of $CuSO_4$ (in triplicates) were used to plot standard curve for each plate used for screen. This helped us confirm the concentration dependent induction of VAP^{P58S}:GFP protein induced in each plate. Second, to ensure the efficiency of dsRNA treatment, dsRNA against VAP and GFP were included in each plate. Third, to also check for reproducibility of the observed phenotype (increase or decrease in percent cells expressing aggregates) post knockdown we chose 4 targets that were repeated across the plates, which could be used as potential controls to check for variation across all plates. For each case if 2 of 3 targets fail to show reproducibility of phenotype, they are marked as false positive (FP) or false negative (FN). If the FP or the FN rates are high for a particular plate, the entire plate is discarded.

High throughput imaging was done using Thermo Array Scan VTI automated station (Figure 6A). 10 fields were imaged per well and 400 cells were imaged per field. Due to presence of triplicates for each sample, around 12000 cells were imaged for each dsRNA knockdown. Dual channel imaging was performed with DAPI labeling each cell nucleus and GFP labeling the mutant VAP aggregates. After Phase-1, we screened for all the genes (~10% *Drosophila* genome) pertaining to the selected categories mentioned in Figure 5 and focused on development of automated programs that could score for percent cells expressing aggregates.

On completion of the analysis, we will perform the secondary screens for the hits obtained from the primary screen on three cell lines – VAP:GFP; GFP and $GFP:VAP^{P58S.}$ In Phase-2, we expect to continue with the rest of the screen with coverage of 50% of Drosophila genome in similar steps.

4. Analysis of the imaged data

The imaged data consists of over 2.5 lakh images including control and test plates. Each well has been imaged using DAPI and GFP channel where both the images are stored in Thermo Array Scan VTI proprietary format (*.C01).

The most challenging part for large high content screening studies has been data analysis. Previous studies have used software packages like MetaMorf to analyze the acquired images (Zhang et al., 2010). Initially, we tried to use commercial software such as Volocity and Cell profiler to identify and count cellular inclusions. These methods were, however, discarded due to limited accessibility to program servers and due to large amount of variation in background noise leading to lack of identification of modifiers that behaved robustly in our pilot screens. Cellular clumps led to difficulty in segmentation for automated analysis software. Due to sheer amount of images (~2.5 lakhs), analyzing these manually was a difficult task.

The *.C01 files were converted using the Bio Format Importer plugin (LOCI; http://loci.wisc.edu/software/bio-formats) or by a custom MATLAB script that would import and process these images. We used both the means to standardize and set up automated analysis. Here, I would be describing the latter, where we developed a MATLAB script for computerized analysis of these aggregates.

Cells were stained with DAPI after fixation to mark the nuclei. Introducing additional steps for processing these samples for optimal imaging decreased the auto-florescence from medium and removed all the floating cells from each field, however it was sometimes seen to introduce debris / small particles in some fields which would lead to problems during automated analysis. Thus, the first step was to detect these debris / particles that had been arising in the well due to manual error during washing or plate errors. Hence, the first part of the code set a size cut-off for the DAPI signal. This meant only particles under acceptable sizes were subjected to further analysis. After iteration of background correction, new images were stored by the code as processed image. The code then read the processed DAPI image and applied K-means clustering by 2 populations assuming each image had pixels with significantly high intensity (florescent DAPI signal) and pixels with lower intensity (background). Once clustered in 2 bins, the high intensity fluorescent pixels were marked as nuclei, such that for each clump of pixels, the peak of the Gaussian curve marked the center of the nucleus of the corresponding cell. S2R+ cells are characterized to be semi-adherent cells with

circular morphology. Under 20x magnification we estimated the cellular radius to be around 10 pixels corresponding to 5 µm. Using this estimate, we dilated each center detected by 10 pixels and obtained Region of interests (ROIs) that represented each cell in the field. Around 400 ROIs were obtained from each field consistent with manually counted cells in these images. Although cells were seeded with a confluency of around 30% in each field, clumping was observed due to overgrowth of cells or during fixation and washing of samples. Since we were interested in identifying the percent cells expressing aggregates, clumped cells posed a big problem. Using ROIs generated, we uniquely labeled each cell and checked for intersection between these ROIs. If areas of any two ROIs overlap more than 30%, the ROIs were marked as a clump and all the connected pixels / ROIs corresponding to clumped cells were deleted from the image.

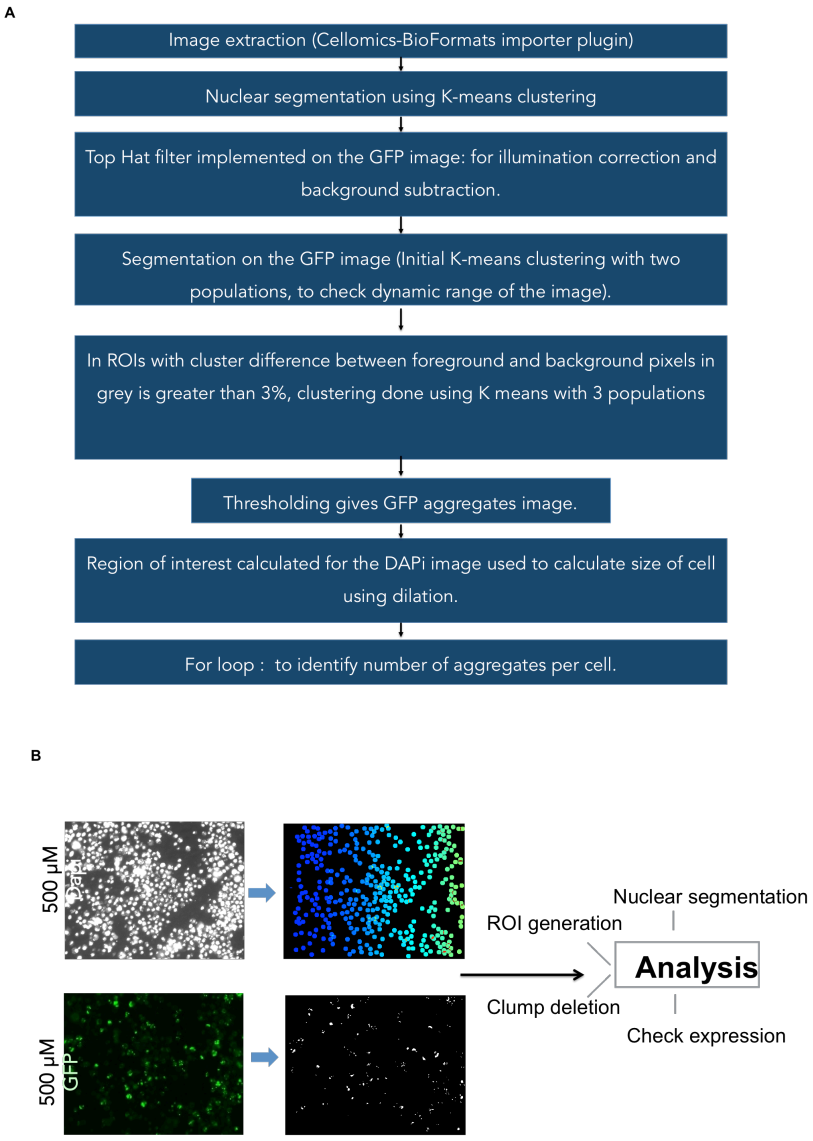

Figure 7: Image Analysis.
A. Workflow of the steps executed for image analysis for the screen. All Images were analysed in an automated manner using MATLAB codes.
B. Representative image for DAPI and GFP being processed to acquire various features that are analysed by the MATLAB code.

To isolate background noise that was intrinsically present in the system we needed to delete the background intensity from each pixel, making all the background pixels to have zero value. However, since auto focus feature during imaging was used on GFP channel that marked aggregates, many DAPI images appeared to be at a small off-set (in z-axis), although they could be identified and quantified. To optimize background correction, we generated another ROI by dilating the radius by a bigger circle that encompasses the entire cell along with few pixels surrounding cells. This was marked as ROI-2 that would quantify the background noise in each image. Thus using DAPI, clumps are deleted, cells are marked as ROIs and ROI-2 is marked for background correction. GFP image is read and pixels are scanned only in regions corresponding to area covered by ROIs. To ensure optimal threshold conditions for each image due to varying background noise we used variable cut-off that was calculated based on background in each image rather than arbitrary fixed cut-off value.

Standard deviation for background in each image was calculated and thresholding was performed after background correction by subtracting mean + 10 times SD of background intensity (obtained from ROI-2), allowing aggregates to be highlighted for efficient counting. K-means clustering of 2 populations was applied on the thresholded image to check for GFP aggregates in each cell. The output file thus contained the following parameters: position of the image in the 384 well plate, field of image, total number of cells, percent cells expressing aggregates, mean GFP intensity for ROIs, standard deviation for GFP intensity in the ROIs and the cut-off value.

Upon identification of percent cells expressing aggregates, another code was written to compile and average the randomly arranged triplicate data corresponding to a single gene. Due to the presence of noise in the system, genes that would show changes in 2 of the total 3 replicates were marked as hits.

The second method used to screen for hits from the screen used a more robust methodology by accounting for inherent variability in the population of screened cells. Similar to the first code, this also used DAPI image to remove non-specific / noisy particles that were picked up in the images, mark cellular nuclei and their corresponding cells and to remove clumps in each field. Average GFP for each cell and total GFP intensity for each well were measured from the DAPI channel generated ROIs and plots for population distribution for both these cases were plotted and compared for each target knockdown. Kolmogorov-Smirnov-like (KS) statistic was used to assign Z-scores to each gene on plate as reported by (Dey et al., 2014) for their whole genome RNAi screen analysis – "*Exploiting Cell-To-Cell Variability To Detect Cellular Perturbations*." Negative and positive control wells could be distinguished after normalization of mean and variance in each plate from their resulting population distribution. Results obtained from the method are shown in Table 1 and discussed in the next section.

5. A list of modifiers of aggregation identified using the screen.

Two independent methods were used to generate a list of modifiers in our screens. Since the list is an output of our primary screen, with secondary screening to follow, we decided to set non-stringent thresholds so as not to lose important modifiers. **Table 1** lists the modifiers using the Analysis method of Dey et. al. (Dey et al., 2014). The methodology for the other method is being refined and the list is a work in progress.

Table 1: List of genes that modify kinetics of aggregation in VAP^{P58S}:GFP. The genes are a small subset (4.8%) of the 1200 screened genes. The genes in bold are known ALS causing loci in humans.

Modifiers	Name of Protein/Gene
CG9543	Coat Protein (coatomer) epsilon
CG9347	neither inactivation nor afterpotential B
CG9324	Pomp
CG9291	Elongin C
CG8998	Regulator of cullins 2
CG8979	-
CG8846	Thor
CG8771	-
CG8532	liquid facets

CG8465	lethal (1) G0222
CG8219	
CG8203	Cyclin-dependent kinase 5
CG8057	alicorn
CG7842	bad egg
CG7504	-
CG7158	**Amyotrophic lateral sclerosis 2 ortholog**
CG6885	-
CG6502	Enhancer of zeste
CG6349	DNA polymerase alpha 180kD
CG6345	-
CG6302	lethal (Li et al.) 01239
CG6147	Tsc1
CG5953	-
CG5841	mind bomb 1
CG5808	-
CG5686	chico
CG5520	Glycoprotein 93
CG5387	Cdk5 activator-like protein
CG5285	-
CG5198	hole-in-one
CG5092	Target of rapamycin
CG4886	cyclophilin-33
CG4627	-
CG4319	reaper
CG3412	supernumerary limbs
CG3411	blistered
CG31098	-
CG3060	morula
CG3051	AMP-activated protein kinase alpha subunit
CG1768	diaphanous
CG1747	Sphingosine kinase 1
CG1736	Proteasome alpha3 subunit, Testis-specific
CG17051	dodo
CG15433	Elongator complex protein 3
CG14490	-
CG13296	-
CG1318	Hexosaminidase 1
CG12919	eiger
CG12423	-
CG11940	pico
CG11793	**Superoxide dismutase**
CG11777	-
CG11335	lysyl oxidase-like
CG11115	Suppressor of Stem-Loop mutation ortholog

	(S. cerevisiae)
CG1100	Regulatory particle non-ATPase 5
CG10956	Serpin 53F
CG1081	Ras homolog enriched in brain ortholog (H. sapiens)
CG1063	Inositol 1,4,5,-tris-phosphate receptor
CG10327	**TAR DNA-binding protein-43 homolog**

The list contains a number of interesting targets, including *Tor, Tuberous Sclerosis Complex 1,Thor* discovered earlier in a fly based genetic screen (Deivasigamani et al., 2014), ALS causative loci (ALS1, ALS2, ALS10) and a dozen genes that are defined as ALS-related (Abel et al., 2012). As we plan our secondary screen, where we will use the hits obtained from Analysis Methods 1 & 2 and test these as modifiers of VAP:GFP and GFP, we have taken a few interesting modifiers and have initiated the downstream process of validation and characterization.

6. Validation of SOD1, Alsin & TBPH -targets discovered in our high throughput screen.

An interesting finding from the list of aggregation modifiers was the identification of other ALS loci such as *Alsin, SOD1* and *TBPH* as modifiers (**Table 1**, highlighted in bold; **Table 2**). **Table 3** lists a few of the ALS-related loci found in our screen (Abel et al., 2012). This result is reminiscent of the observations made using a reverse genetic screen that was used to identify genetic modifiers of VAP (Deivasigamani et al., 2014). This fly based screen, using reduced macrochaetae of the Dorsal thorax of flies as a sensitized genetic background (seen in *Sca-Gal4 > UAS-VAP*) was used to identify amongst 102 modifiers, the ALS genes *SOD1, Alsin* and *TBPH*. The same players are significant hits in a completely independent experiment in S2 cells, using VAP^{P58S}:GFP aggregation as a readout. This result strongly suggests a gene regulatory network of VAP modifiers that exists in cells (including neurons) with both VAP and VAP^{P58S}. The elements of this network (VAP, Alsin, SOD1, TBPH) appear to be sensitive to each other's activity.

Table 2: List of ALS causative loci that modify kinetics of aggregation in VAP^{P58S}:GFP.

Gene		Name	Chromosome	Function
Alsin	ALS2	Amyotrophic lateral sclerosis 2 ortholog	2q33.2	Rab guanyl-nucleotide exchange factor activity
SOD1	ALS1	Superoxide dismutase	21q22.11	antioxidant activity
TARDBP/ TDP43	ALS10	TAR DNA-binding protein-43 homolog	1p36.22	mRNA binding and processing

Table 3: List of ALS-related genes that modify kinetics of aggregation in VAP^{P58S}:GFP. Six of the fourteen genes that are identified as modifiers of aggregation in our screen. The ninetten genes are defined as ALS-related genes by the ALSoD database (Abel et al., 2012).

ITPR2		Inositol 1,4,5,-tris-phosphate receptor	12p11.23	Calcium channel activity
AGT		Serpin 53F	1q42-q43	Serine-type endopeptidase inhibitor activity
LOX		lysyl oxidase-like	5q23.2	Scavenger receptor activity
HEXA		Hexosaminidase 1	15q23	beta-N-acetylglucosaminidase activity
ELP3		Elongator complex protein 3	8p21.1	acetyltransferase activity
DIAPH3		diaphanous	13q21.2	Rho GTPase binding

We validated *SOD1, Alsin* and *TBPH* by repeating the high throughput experiments in-house in 96 well imaging plates, visualizing the aggregates using EVOS FL Auto microscope. Our results confirmed the trends seen in our screen; that knockdown of *SOD1* decreased the formation of VAP^{P58S}:GFP aggregates while *Alsin* and *TBPH* knockdown led to an increase in aggregate formation. In order to further understand the effect on VAP^{P58S}:GFP levels, we utilized western blots to monitor the change in protein levels on SOD1, Alsin and TBPH

knockdown.

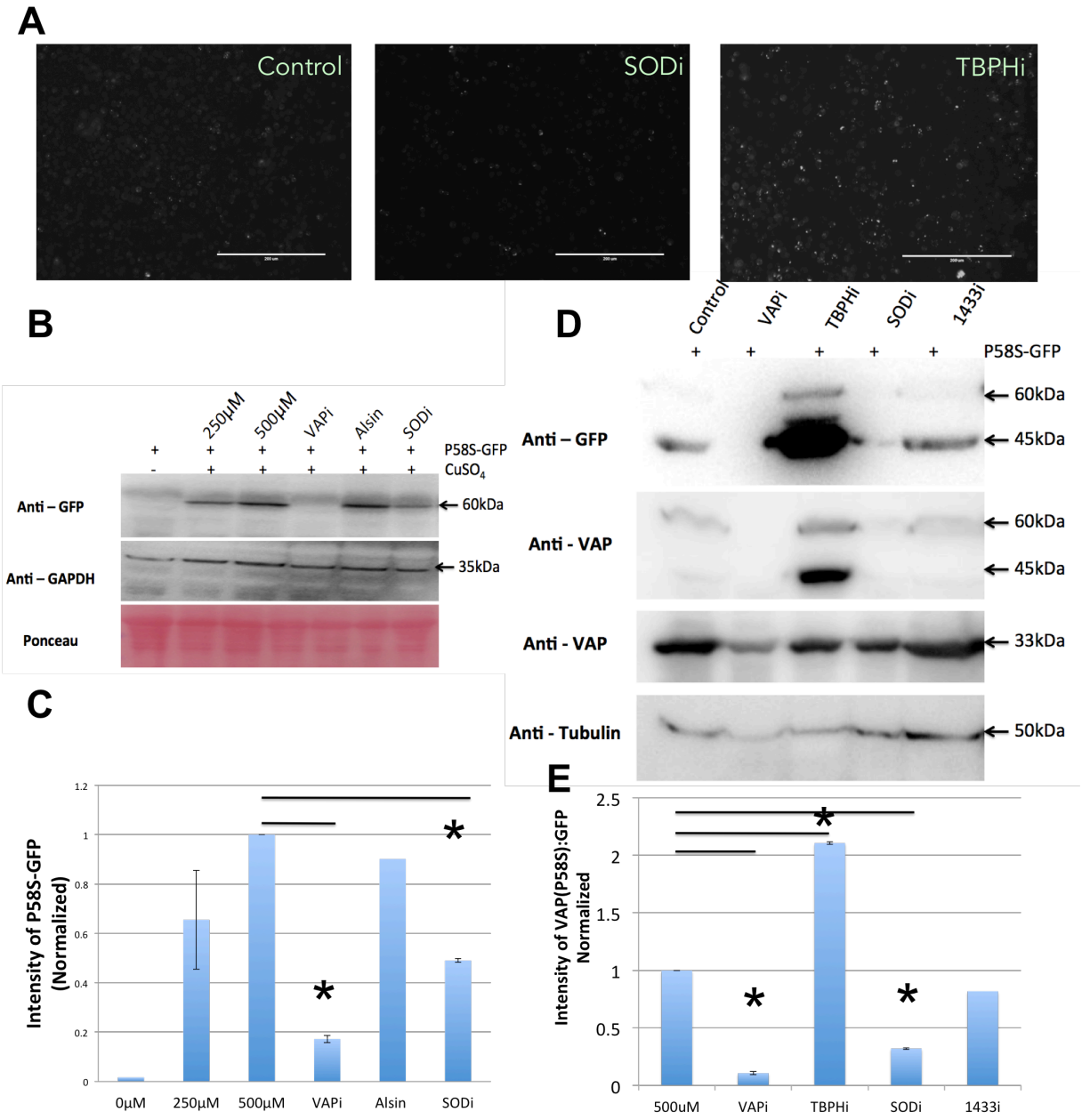

Figure 8: Validation. Knockdown of modifiers (SOD1, TBPH, Alsin) changes kinetics of aggregation.

A. Images acquired from EVOS microscope under 20x for Mock, *TBPH* and SOD1 knockdown. SOD1i shows reduced number of cells expressing aggregates whereas TBPHi shows an increase in number of cells expressing. dsRNA for these experiments was made in-house using clones procured from the DGRC Gold collection.

B. Western blots indicate that knockdown of SOD1 leads to a decrease of VAP^{P58S}:GFP levels, equivalent to a two-fold reduction (250 µM) of protein expression while Alsin levels do not change significantly.

C. Quantification for the western blot. Values normalized with intensity of GAPDH and further normalized to control. (Error bars indicate SD; N=3) (* Indicates p-value less than 0.001)

D. Unlike in the case of SOD1 knockdown, knockdown of TBPH increases VAP^{P58S}:GFP levels. An intense protein band is also seen at 45 kDa, suggesting a N-terminal deletion in VAP, possibly the MSP domain.

E. Quantification for the western blot. Values normalized with intensity of Tubulin and further normalized to control. (Error bars indicate SD; N=3) (***** Indicates p-value less than 0.001)

As shown in **Figure 8**, knockdown of *SOD1* decreased the levels of VAP^{P58S}:GFP (a 60 kDa band) by 50% as compared to a VAP knockdown, that decreased levels by 80%. VAP^{P58S}:GFP levels increased by 100% on knockdown of TBPH, which led to an increase in VAP^{P58S} aggregates. Interestingly, the most dramatic change was the increase in a cross-reactive band at 45 kDa. Based on its size and cross-reactivity to the anti-VAP (CCD domain) antibody, we predict that this may correspond to cleaved VAP^{P58S}:GFP without the MSP domain.

7. SOD1 knockdowns lead to a decrease in VAP aggregation.

One of the key findings from our screen was that knockdown of *Super-oxide Dismutase (SOD1)* led to 40% decrease in cells expressing VAP^{P58S}:GFP aggregates. The phenotype was reproducible and statistically significant. SOD1 was the first genetic loci identified in ALS. Multiple mutations in the wild type SOD1 protein have been reported to lead to misfolding and aggregation and the manifestation of ALS. It has been reported that VAP levels are reduced in mice ALS models of mutant SOD1 background (Teuling et al., 2007). Here, we report the perturbations of mutant VAP^{P58S}:GFP levels upon decrease in *SOD1* activity by RNAi.

As shown in Figure 8, using western blots, we validated the levels of VAP^{P58S}:GFP levels in the SOD1 knockdown background. Consistent with the screen data, we detected lowered protein levels of mutant VAP^{P58S}:GFP in western blots. To further check for effect of SOD1 dsRNA on metallothionein promoter, we checked the effect of SOD1 dsRNA on VAP:GFP and GFP alone. No change was seen on VAP:GFP or GFP protein levels on SOD1 knockdown in the respective cell lines (Data not shown) indicating that the effect was specific to the aggregation prone form of VAP.

Further we checked the effect on aggregation of VAP^{P58S}:GFP upon overexpression of SOD1. Epi-fluorescence images did not show a significant up regulation in aggregate expressing cells. However western blotting showed an increase in VAP^{P58S}:GFP levels upon over expression of SOD1 in S2R+ cells

(**Figure 9**). The experiments are preliminary and need to be repeated with different loading controls.

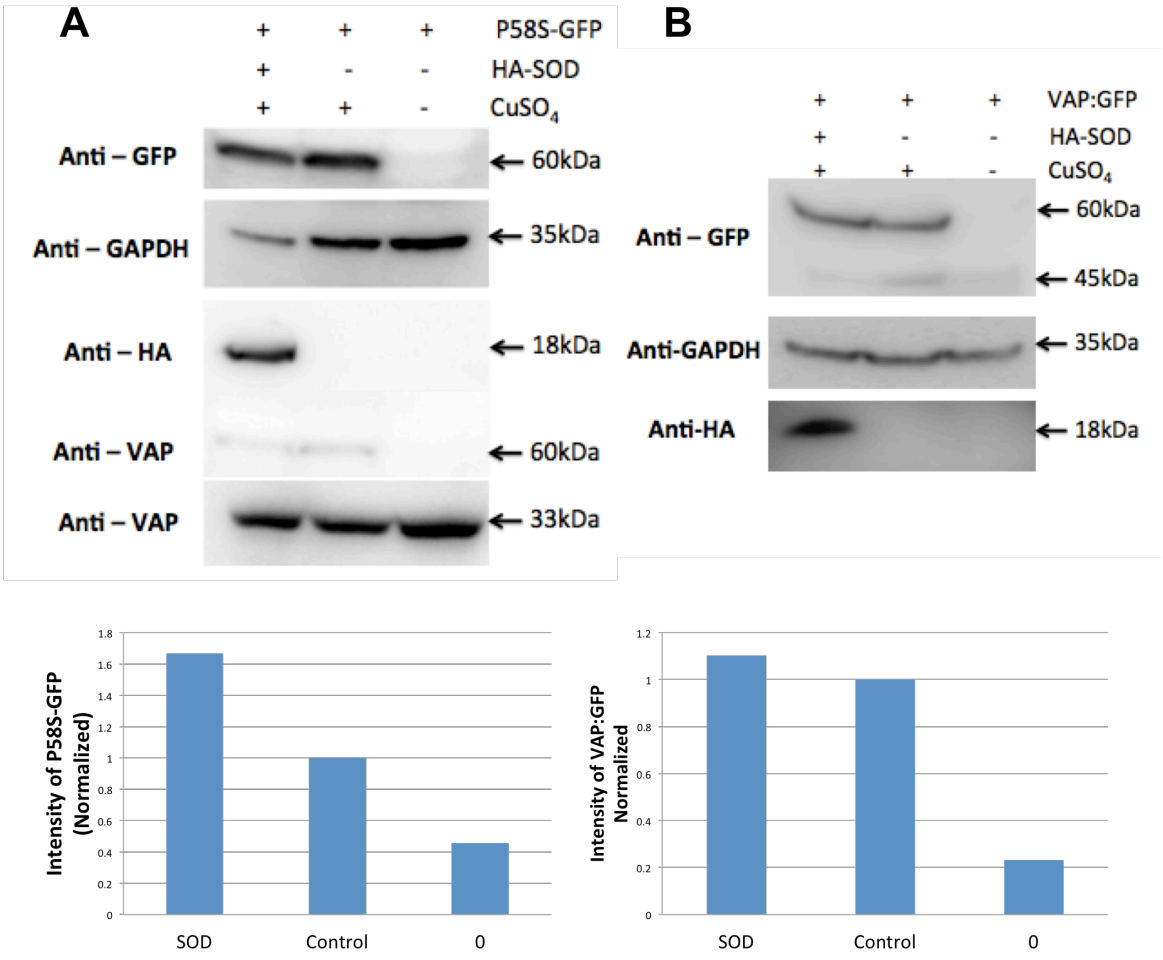

Figure 9: **Overexpression of SOD modify VAP^{P58S}:GFP levels but not VAP protein levels.**
A. Protein levels of mutant VAP are changed on expression of SOD-HA. However, SOD overexpression fails to modify levels of wildtype VAP.
B. Quantitation of band intensity in western blots using Image-J indicates an increase in VAP^{P58S}:GFP but no change in VAP:GFP on overexpression of SOD1.(N=2)

The most striking phenotype being the decreased aggregation of VAP^{P58S}:GFP in S2 cells; the same experiment was carried out in flies, with change in aggregation of untagged VAP^{P58S} measured in larval brain tissue. As shown in **Figure 10**, in fly brains with overexpressed VAP^{P58S}, aggregates are formed with numbers dependent on level of VAP^{P58S} expression, which more at 25 °C as compared to 18 °C, based on temperature dependent Gal4

expression.

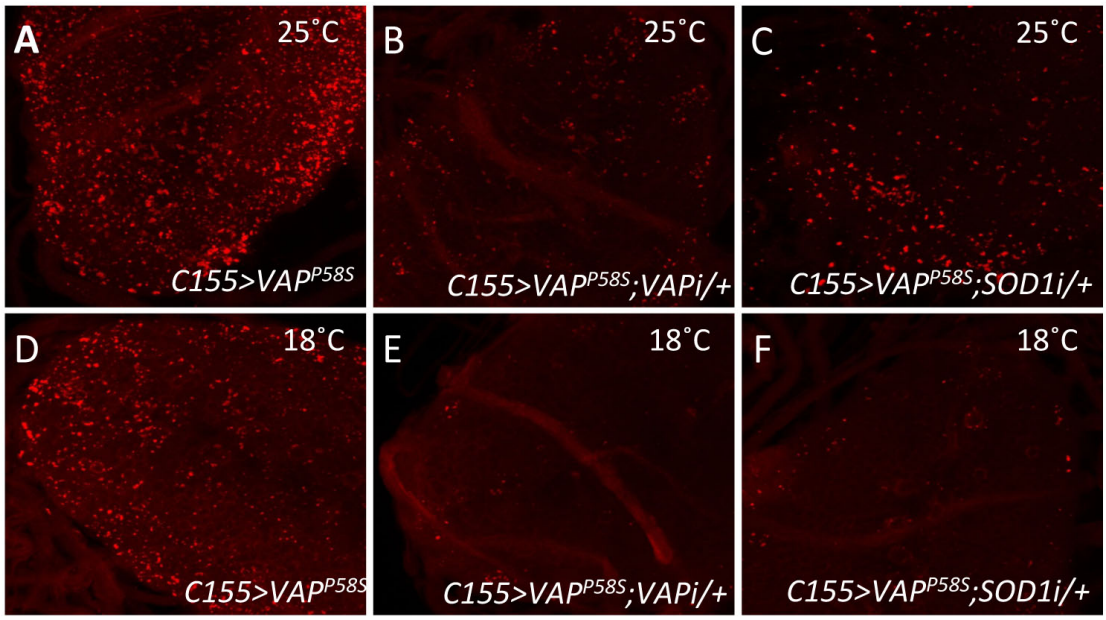

Figure 10: Knockdown of SOD1 in *Drosophila* brain decrease VAP^{P58S} aggregate formation.
Representative images of expression of mutant VAP-P58S aggregates driven by pan-neuronal *C155-Gal4* at 25˚C (A) and 18˚C (D) in the ventral nerve cord, immunostained with rabbit anti-CCD (VAP) antibody and imaged using Zeiss 710 confocal microscope. Knockdown of VAP leads to dramatic decrease in number of aggregates (B and E) as compared to *C155>VAP^{P58S}* control (A and D). Knockdown of *SOD1* leads to considerable decrease in number of aggregates (C and F) as compared to *C155>VAP^{P58S}* control (A and D). This knockdown however is not as dramatic as *VAP* knockdown (B and E). Figure contributed by Kriti Chaplot.

Knockdown of *VAP* transcripts by RNAi (**Figure 10 B & E**) leads to a reduction of expressed protein and thus reduction of number of aggregates. Similarly, reduction of *SOD1* transcripts also led to reduction in VAP^{P58S} aggregates. This result, in a cell type different from S2R+ cells, confirms that VAP^{P58S} protein/aggregate levels are sensitive to SOD1 activity and these levels fall with decrease in *SOD1*.

8. Decrease in VAP aggregation may be a response to increased ROS.

The decrease in aggregation for VAP^{P58S}:GFP on knockdown of SOD1 is intriguing. A primary function for SOD1 in the cell is the regulation of superoxide radicals (Muller et al., 2006). SOD1 reduces super oxides to peroxide (H_20_2) and water. One effect of malfunction or reduction of SOD1 activity would

be an increase in superoxide levels in the cell.

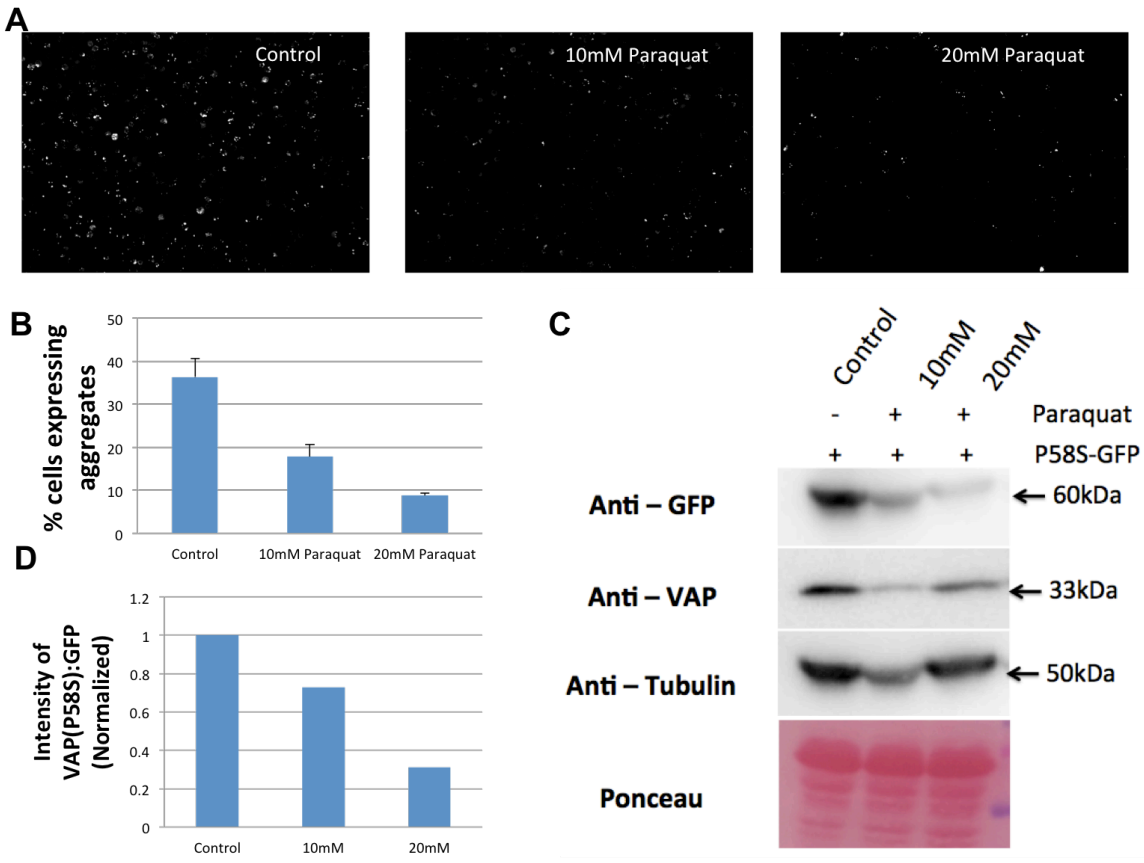

Figure 11: Decrease in aggregation of VAP^{P58S} may be a result of increased ROS in cells.
A. Paraquat, a chemical used to induce production of ROS species in cells, when added to the VAP^{P58S}:GFP stable line appears to lead to a decrease of cells with aggregates. Cells expressing VAP^{P58S}:GFP were treated with 10mM and 20mM Paraquat for 24 hrs prior to induction with 500uM CuSO4. Trypan Blue assay was used to account for cell death. Cell viability was estimated to be 97% for control and 92.8% and 92.3% for 10mM and 20mM treatment with Paraquat respectively. The samples were then processed for westerns.
B. Quantitation of percent cells with aggregates indicates a 2.5 fold decrease at 20 mM Paraquat. (Error bars indicate SD) (cells counted =1000)
C. Western blots of cells treated with Paraquat indicate a decrease in both VAP and VAP^{P58S}:GFP protein levels, which in turn would account for a decrease in aggregates.
D. Quantitation of the western blots, showing 2-3 fold decrease in VAP^{P58S} levels on addition of Paraquat to cellular media. (N=2)

An independent method to increase superoxide levels without perturbing SOD1 levels is the addition of the chemical agent Paraquat (Oeda et al., 2001). In order to test if the decrease of aggregates of VAP^{P58S} was indeed in response to increased superoxide levels, we added Paraquat to the liquid media. Increasing amounts of Paraquat 10mM and 20mM (**Figure 11-A, B**) lead to 30% and 70%

decrease of percent aggregation in the VAP^{P58S}:GFP line respectively (p-value 0.003 and 0.0004 respectively), which appeared to be because of decrease in VAP^{P58S}:GFP protein levels (**Figure 11-C**). This result appears to confirm that the decrease in VAP levels is an effect of increase superoxide levels. Though this data is interesting, we do not, as of now, have a mechanistic understanding of the relationship between these two events.

Discussion

In the era of high throughput genomic screens, S2 cells have been the primary workhorses for many cell based genetic screens (Agaisse et al., 2005; Boutros et al., 2004; D'Ambrosio and Vale, 2010; Goshima et al., 2007; Nybakken et al., 2005). Over a hundred genomic screens have been carried out by the Harvard based *Drosophila* RNAi Screening Centre alone (DSRC) (Flockhart et al., 2012). Recent developments in the field of imaging and microscopy coupled to genetics have encouraged the use of high-throughput cell-based screens to identify genes responsible for complex cellular pathways. However, only a limited number of screens have been performed to identify modifiers of aggregation underlying neurodegenerative disorders. Initial screens (Teuling et al., 2011; Zhang et al., 2010) examined the effect of knocking down of genes on aggregates in *Drosophila melanogaster* tissue culture cells and also in human cells respectively. High throughput RNAi screening techniques along with automated image acquisition has identified image analysis a rate-limiting step in most of these studies.

In this study using an RNAi knockdown strategy we successfully report an assay to identify modifiers of VAP^{P58S} aggregation in S2R+ cells. The methodlogy is based on earlier screens, with the change that we use a VAP^{P58S}:GFP fusion to visualize aggregates by epifluorescence. Of the 1200 genes screened we find that 58 genes that on knockdown modifiy aggregation. These 58 genes need to be validated through the planned secondary screens using VAP:GFP and GFP cell lines. Validation steps allow us to rule out non-specific effects that are not related to specific modification of VAP^{P58S} aggregation kinetics.

As of 2015, 26 loci have been identified that are affected or involved in ALS. These include proteins like SOD1, TDP-43, Alsin, Ataxin, VAP that are involved in varied cellular processes. It is yet unclear how single or multiple point mutations in one or more than one of these loci lead to the same disease. We hypothesize that there might be a pathway by which these genes might be interconnected and perturbation of this pathway can lead to the disease. The 1200 genes we screened contain 56 ALS loci, contributing to 4% of screened

targets. We find that 17 genes (15% of identified hits) affected aggregation kinetics, thus supporting our hypothesis. The 17 genes however need to be validated and intercations shown to have biological significance either for cellular homeostasis or disease.

The most common mutant of SOD1 protein, G93A has been shown to aggregate and form intracellular inclusions. C. Hoogenraad and group have reported perturbation of wild-type VAP levels in mutant SOD1 cases using mouse as model system (Teuling et al., 2007). However, no one has yet reported the effect of SOD1 knockdown on mutant VAP levels conditions. We here show evidence that VAP^{P58S} levels might be regulated by SOD1 levels leading towards a possible cross talk between these ALS causing loci. We had also screened for genes pertaining to categories like autophagy (117 genes contributing to 9% of total screened genes) and ubiquitin proteasome pathway (98 genes contributing to 7% of screened genes). We identified 5 genes and 19 genes corresponding to 4% and 17% of identified hit list that are involved in autophagy and UPS pathway. Inclusion bodies in ALS have been shown to co-localize with proteins like ubiquitin, p62 and chaperones leading researchers to believe that Ubiquitin proteasome system (UPS) and autophagy-lysosome system plays a vital role in clearing or containing the aggregated proteins (Blokhuis et al., 2013).

In this study we have have also validated one target from the screen, namely SOD1. As shown in results, SOD1 knockdowns appear to reduce the levels of VAP^{P58S}:GFP protein the cells and thus reduces levels of aggregates. This affect is interesting, especialy considering that transcription is driven not by a native promoter but by a metallothionein promoter that is constitutively active. This strongly suggests that the decrease in protein levels is a post-transcriptional response, possibly because of increased turnover of the protein by cellular pathways that degrade the soluble or aggregated protein. SOD1 functions in the cell to regulate the levels of superoxides which are a by product of mitochondrial physiology and are toxic to cells if not contained. One effect of SOD1 knockdown is the increase in superoxide levels in the cell, which in turn may lead to the increased turnover of proteins in general or VAP^{P58S} in particular. We tested the relationship between VAP^{P58S} reduction and superoxide levels by inducing

superoxide levels, without knocking down SOD1 using the chemical agent paraquat. Paraquat addition to the culture media led to a dramatic decrease in both VAP^{P58S} protein levels as also aggregation. This suggests a mechanistic link between SOD1 and VAP^{P58S} via levels of cellular superoxides.

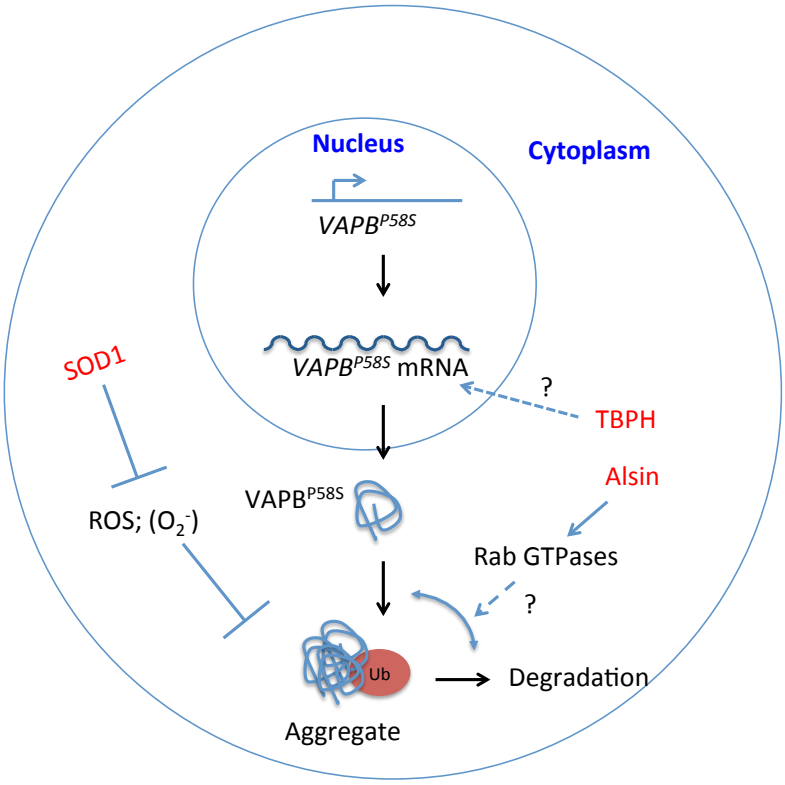

Figure 12: A mechanistic model for the interaction of *VAPB^{P58S}* with *SOD1* ,*TBPH* and *Alsin*.
Our data indicates that VAPB^{P58S} aggregates are affected by both SOD1, a cytoplasmic protein with antioxidant function as well as TBPH, a protein implicated in mRNA binding and processing. Our data suggests that VAPB^{P58S} aggregate formation is sensitive to superoxide levels in the cell, based on data from *SOD1* knockdown and paraquat treatment. The mechanism for the effect of TBPH on VAPB^{P58S} aggregate formation in unknown and may involve regulation of VAPB mRNA. Alsin has not been well characterized, with possible roles as a Rab GTPase regulator. Its role in modifying VAPB^{P58S} aggregation may be via regulation of endosomal trafficking.

Mutations in Alsin gene have been implicated to lead to juvenile recessive form of ALS2. Alsin is an activator for small GTPase Rab5, which is involved in endosomal dynamics (Kunita et al., 2007). The 2015 study using Drosophila as a model system, reports abnormal accumulation of Rab5 proteins in eye imaginal discs in background of expression of mutant VAP protein (Sanhueza et al., 2015). Alsin could thus be regulating aggregation of VAP^{P58S} by perturbing levels of Rab5.

The Drosophila homologue for TDP-43 (Tar DNA binding protein-43) is TBPH that is associated with ALS. TDP-43 is conserved ubiquitously expressed protein that has been shown to contain multiple RNA binding motifs that are involved in mRNA splicing, transcription, stability and transport. Perturbing levels of wild type TBPH in flies has been reported to lead to key neurological disorders like motor defects, decreased life span (Diaper et al., 2013b). In brains of patients with ALS, FLTD and Alzheimer's, TDP-43 positive inclusions have been observed in the cytoplasm. Transgenic mice expressing ALS8 associated VAP^{P56S} are shown to develop cytoplasmic TDP-43 and ubiquitin positive aggregates in motor neurons (Tudor et al., 2010).

In summary, I have successfully established a Schneider cell based system for a high throughput screen that can identify modifiers of ALS8 cellular inclusions. Methodlogy for knockdown and imaging has been standardized and 1200 genes have been tested in the first phase of the proposed whole genome screen. Various methods have been explored for analysis of the imaged data so as to extract information on modifiers of VAP^{P58S}. This entire effort establishes the protocols developed as a useful way to understand neuroaggregation. A key result is the identification of other ALS loci as modifiers, especially SOD1. A mechanistic exploration of the dependancies of different ALS loci on each other using cellular and animal models, as planned in our study should lead to a better understanding of initiation and progression of ALS in humans.

Appendix

MATLAB Code used for Image Processing and Analysis

```
wellvec=('A','B','C','D','E','F','G','H','I','J','K','L','M','N','O','P');
slashtype='/';                                          %dependent on OS.
nucleiSize = 30;
LargeObjSize = 300;

idx1=findstr(slashtype,inputdir);                       %ResultMat
cc=date; cc = strrep(cc, '-', '');
resultmat = [inputdir(idx1(end)+1:end) '_' cc '.mat'] %Output analyzed file

filepath=fuf([inputdir slashtype '*.C01'],'detail');  %Path
filepath=filepath{1};
reader = bfopen(filepath);

welldatamat=[];namevec={};frac_agg=[];frag_ratio=[];
for i=1:size(reader,1)                                  %length(reader)-1

    series1 = reader{i,1};

    gfp1=series1{2,1};                                  %Read GFP
    gfp=double(imtophat(gfp1,strel('disk',12)));

    dapi=series1{1,1};                                  %Read DAPI
    dapimain = dapi;
    dapi = double(imtophat(dapi,strel('disk',60)));

    wellsrch='Well ';                                   %Map Well-ID
    metadata=series1{1,2};
    idx1=findstr(wellsrch,metadata);
    wellid=metadata(idx1(end)+length(wellsrch):idx1(end)+length(wellsrch)+2);
    wellx=strmatch(wellid(1),wellvec,'exact');
    welly=str2double(wellid(2:3));

    fieldsrch='Field #';                                %FieldID
    idx2=findstr(fieldsrch,metadata);

fieldnumber=str2double(metadata(idx2(end)+length(fieldsrch):idx2(end)+length(fie
ldsrch)+1));


    f= im2bw(mat2gray(double(dapi)), 0.2);              %Cluster 20% highest
pixels
    f = bwareaopen(f,60);
    f = ~f;
    dapi = double(dapi).*f;
                                          % Florescent and background on DAPI
    [aa ii]=kmeans(double(dapi(:)),2,'emptyaction','singleton');


    linvec1=dapi(:);               % finds minimum pixel intensity of each class
    threshvec=[min(linvec1(aa==1)) min(linvec1(aa==2))];

    img1=dapi>max(threshvec);     % marks that class that has maximum intensity
    img2=bwareaopen(bwlabel(img1),LargeObjSize);

    pixidx=intersect(find(img1==1),find(img2==0))    % removes cell clumping
    finimg=zeros(size(dapi,1),size(dapi,2));
    finimg(pixidx)=1;

    nfinimgd = zeros(size(dapi,1),size(dapi,2));
    npixid1= intersect(find(img1==0),find(dapi==1));
    nfinimgd(npixid1)=1;

    finimg=imclearborder(bwareaopen(finimg,nucleiSize)); %filter through cells
```

```
     centvec=regionprops(bwlabel(finimg),'Centroid','Area'); %Threshold GFP
     zerovec1=zeros(size(dapi,1),size(dapi,2));
     zerovec31=zerovec1;
     gfp_img=zerovec1;tmpimg=zerovec1;
     ag_idx=1;
     for z=1:length(centvec)

            zerovec=zeros(size(dapi,1),size(dapi,2));     %make and empty image
            idx=z;
                                                % round centroids to integers
zerovec(round(centvec(idx).Centroid(2)),round(centvec(idx).Centroid(1)))=1;
            zerovec=imdilate(zerovec,strel('disk',11));   %generate ROI by 11
            zerovec3=imdilate(zerovec,strel('disk',30));  %negative area ROI
            idx2=find(zerovec>0);
            nidx2 = find(zerovec3>0);
            zerovec3(nidx2)=z;                            %negative ROI
            zerovec(idx2)=z;
            zerovec1=zerovec1+zerovec;
            zerovec31 = zerovec31+zerovec3;               %negative ROI cutoff
            clear nidx2 idx2 idx;

     end

     clear negpixid;
     negpixid=intersect(find(nfinimgd==1),find(zerovec31==0));
     clear jj;
     jj=gfp(negpixid);
     cutoff=mean(jj)+10*std(jj);
     cutoff2 = mean(jj)+5*std(jj);
     clear idx2 idx3;

        img1=gfp>cutoff;                              %thresholding by z-score
        t_img1=gfp>cutoff2;
        img2=bwareaopen(bwlabel(img1),10);
        img3=bwareaopen(bwlabel(img1),150);

        t_img3=bwareaopen(bwlabel(t_img1),150);
        pixidx=setdiff(find(img2==1),find(img3==1));
        finimg1=img2;
        finimg2=zeros(size(gfp,1),size(gfp,2));
        finimg2(pixidx) = 1;

    img1=finimg1;

           idx3=intersect(find(zerovec1>0),find(finimg2>0));
           gfp_img(idx3)=gfp(idx3);

           line_gfp = double(gfp(:));
           lin_gfp_img = line_gfp(idx3);

           agr_img=zerovec1(idx3);
           aggregates(i,1)=length(unique(agr_img))-1;
           total_cells (i,1) = z;
           welldatamat(i,:) = [total_cells(i,1), wellx, welly, fieldnumber,
aggregates(i,1),mean(lin_gfp_img),std(lin_gfp_img),mean(jj),cutoff];
           namevec=[namevec ; [wellid '_' num2str(fieldnumber)]];
           mat_cell(wellx,welly) = mat_cell(wellx,welly)+total_cells(i,1);
           mat_ag(wellx,welly) = mat_ag(wellx,welly)+aggregates(i,1)
 end

plate(counter,1).matcell = mat_cell;
plate(counter,1).matag = mat_ag;
plate(counter,1).matratio = mat_ag./mat_cell;
save(resultmat,'welldatamat','namevec','plate');
end
```

References

1. Abel, O., Powell, J.F., Andersen, P.M., and Al-Chalabi, A. (2012). ALSoD: A user-friendly online bioinformatics tool for amyotrophic lateral sclerosis genetics. Human mutation *33*, 1345-1351.
2. Andersen, P.M., and Al-Chalabi, A. (2011). Clinical genetics of amyotrophic lateral sclerosis: what do we really know? Nature reviews Neurology *7*, 603-615.
3. Bier, E. (2005). Drosophila, the golden bug, emerges as a tool for human genetics. Nat Rev Genet *6*, 9-23.
4. Blokhuis, A.M., Groen, E.J., Koppers, M., van den Berg, L.H., and Pasterkamp, R.J. (2013). Protein aggregation in amyotrophic lateral sclerosis. Acta neuropathologica *125*, 777-794.
5. Chai, A., Withers, J., Koh, Y.H., Parry, K., Bao, H., Zhang, B., Budnik, V., and Pennetta, G. (2008). hVAPB, the causative gene of a heterogeneous group of motor neuron diseases in humans, is functionally interchangeable with its Drosophila homologue DVAP-33A at the neuromuscular junction. Human molecular genetics *17*, 266-280.
6. Chhangani, D., and Mishra, A. (2013). Protein Quality Control System in Neurodegeneration: A Healing Company Hard to Beat but Failure is Fatal. Mol Neurobiol.
7. Chiu, A.Y., Zhai, P., Dal Canto, M.C., Peters, T.M., Kwon, Y.W., Prattis, S.M., and Gurney, M.E. (1995). Age-dependent penetrance of disease in a transgenic mouse model of familial amyotrophic lateral sclerosis. Mol Cell Neurosci *6*, 349-362.
8. Cleveland, D.W., and Rothstein, J.D. (2001). From Charcot to Lou Gehrig: deciphering selective motor neuron death in ALS. Nat Rev Neurosci *2*, 806-819.
9. Cluskey, S., and Ramsden, D.B. (2001). Mechanisms of neurodegeneration in amyotrophic lateral sclerosis. Mol Pathol *54*, 386-392.
10. D'Ambrosio, M.V., and Vale, R.D. (2010). A whole genome RNAi screen of Drosophila S2 cell spreading performed using automated computational image analysis. The Journal of cell biology *191*, 471-478.
11. Deivasigamani, S., Verma, H.K., Ueda, R., Ratnaparkhi, A., and Ratnaparkhi, G.S. (2014). A genetic screen identifies Tor as an interactor of VAPB in a Drosophila model of amyotrophic lateral sclerosis. Biology open *3*, 1127-1138.
12. Dey, G., Gupta, G.D., Ramalingam, B., Sathe, M., Mayor, S., and Thattai, M. (2014). Exploiting cell-to-cell variability to detect cellular perturbations. PloS one *9*, e90540.
13. Diaper, D.C., Adachi, Y., Lazarou, L., Greenstein, M., Simoes, F.A., Di Domenico, A., Solomon, D.A., Lowe, S., Alsubaie, R., Cheng, D.*, et al.* (2013a). Drosophila TDP-43 dysfunction in glia and muscle cells cause cytological and behavioural phenotypes that characterize ALS and FTLD. Human molecular genetics *22*, 3883-3893.
14. Diaper, D.C., Adachi, Y., Sutcliffe, B., Humphrey, D.M., Elliott, C.J., Stepto, A., Ludlow, Z.N., Vanden Broeck, L., Callaerts, P., Dermaut, B.*, et al.*

(2013b). Loss and gain of Drosophila TDP-43 impair synaptic efficacy and motor control leading to age-related neurodegeneration by loss-of-function phenotypes. Human molecular genetics *22*, 1539-1557.
15. Gkogkas, C., Middleton, S., Kremer, A.M., Wardrope, C., Hannah, M., Gillingwater, T.H., and Skehel, P. (2008). VAPB interacts with and modulates the activity of ATF6. Hum Mol Genet *17*, 1517-1526.
16. Gurney, M.E., Pu, H., Chiu, A.Y., Dal Canto, M.C., Polchow, C.Y., Alexander, D.D., Caliendo, J., Hentati, A., Kwon, Y.W., Deng, H.X.*, et al.* (1994). Motor neuron degeneration in mice that express a human Cu,Zn superoxide dismutase mutation. Science *264*, 1772-1775.
17. Kunita, R., Otomo, A., Mizumura, H., Suzuki-Utsunomiya, K., Hadano, S., and Ikeda, J.E. (2007). The Rab5 activator ALS2/alsin acts as a novel Rac1 effector through Rac1-activated endocytosis. The Journal of biological chemistry *282*, 16599-16611.
18. Lev, S., Ben Halevy, D., Peretti, D., and Dahan, N. (2008). The VAP protein family: from cellular functions to motor neuron disease. Trends Cell Biol *18*, 282-290.
19. Li, Y., Ray, P., Rao, E.J., Shi, C., Guo, W., Chen, X., Woodruff, E.A., 3rd, Fushimi, K., and Wu, J.Y. (2010). A Drosophila model for TDP-43 proteinopathy. Proceedings of the National Academy of Sciences of the United States of America *107*, 3169-3174.
20. Muller, F.L., Song, W., Liu, Y., Chaudhuri, A., Pieke-Dahl, S., Strong, R., Huang, T.T., Epstein, C.J., Roberts, L.J., 2nd, Csete, M.*, et al.* (2006). Absence of CuZn superoxide dismutase leads to elevated oxidative stress and acceleration of age-dependent skeletal muscle atrophy. Free radical biology & medicine *40*, 1993-2004.
21. Mulligan, V.K., and Chakrabartty, A. (2013). Protein misfolding in the late-onset neurodegenerative diseases: Common themes and the unique case of amyotrophic lateral sclerosis. Proteins.
22. Murakami, T., Yang, S.P., Xie, L., Kawano, T., Fu, D., Mukai, A., Bohm, C., Chen, F., Robertson, J., Suzuki, H.*, et al.* (2012). ALS mutations in FUS cause neuronal dysfunction and death in Caenorhabditis elegans by a dominant gain-of-function mechanism. Hum Mol Genet *21*, 1-9.
23. Nishimura, A.L., Mitne-Neto, M., Silva, H.C., Richieri-Costa, A., Middleton, S., Cascio, D., Kok, F., Oliveira, J.R., Gillingwater, T., Webb, J.*, et al.* (2004). A mutation in the vesicle-trafficking protein VAPB causes late-onset spinal muscular atrophy and amyotrophic lateral sclerosis. Am J Hum Genet *75*, 822-831.
24. Oeda, T., Shimohama, S., Kitagawa, N., Kohno, R., Imura, T., Shibasaki, H., and Ishii, N. (2001). Oxidative stress causes abnormal accumulation of familial amyotrophic lateral sclerosis-related mutant SOD1 in transgenic Caenorhabditis elegans. Human molecular genetics *10*, 2013-2023.
25. Pasinelli, P., and Brown, R.H. (2006). Molecular biology of amyotrophic lateral sclerosis: insights from genetics. Nat Rev Neurosci *7*, 710-723.
26. Pennetta, G., Hiesinger, P.R., Fabian-Fine, R., Meinertzhagen, I.A., and Bellen, H.J. (2002). Drosophila VAP-33A directs bouton formation at neuromuscular junctions in a dosage-dependent manner. Neuron *35*, 291-306.
27. Ratnaparkhi, A., Lawless, G.M., Schweizer, F.E., Golshani, P., and Jackson, G.R. (2008). A Drosophila model of ALS: human ALS-

associated mutation in VAP33A suggests a dominant negative mechanism. PloS one *3*, e2334.
28. Renton, A.E., Chio, A., and Traynor, B.J. (2014). State of play in amyotrophic lateral sclerosis genetics. Nature neuroscience *17*, 17-23.
29. Robberecht, W., and Philips, T. (2013). The changing scene of amyotrophic lateral sclerosis. Nat Rev Neurosci *14*, 248-264.
30. Rosen, D.R., Siddique, T., Patterson, D., Figlewicz, D.A., Sapp, P., Hentati, A., Donaldson, D., Goto, J., O'Regan, J.P., Deng, H.X.*, et al.* (1993). Mutations in Cu/Zn superoxide dismutase gene are associated with familial amyotrophic lateral sclerosis. Nature *362*, 59-62.
31. Sanhueza, M., Chai, A., Smith, C., McCray, B.A., Simpson, T.I., Taylor, J.P., and Pennetta, G. (2015). Network analyses reveal novel aspects of ALS pathogenesis. PLoS genetics *11*, e1005107.
32. Stadler, C., Rexhepaj, E., Singan, V.R., Murphy, R.F., Pepperkok, R., Uhlen, M., Simpson, J.C., and Lundberg, E. (2013). Immunofluorescence and fluorescent-protein tagging show high correlation for protein localization in mammalian cells. Nature methods *10*, 315-323.
33. Tarasiuk, J., Kulakowska, A., Drozdowski, W., Kornhuber, J., and Lewczuk, P. (2012). CSF markers in amyotrophic lateral sclerosis. J Neural Transm *119*, 747-757.
34. Teuling, E., Ahmed, S., Haasdijk, E., Demmers, J., Steinmetz, M.O., Akhmanova, A., Jaarsma, D., and Hoogenraad, C.C. (2007). Motor neuron disease-associated mutant vesicle-associated membrane protein-associated protein (VAP) B recruits wild-type VAPs into endoplasmic reticulum-derived tubular aggregates. The Journal of neuroscience : the official journal of the Society for Neuroscience *27*, 9801-9815.
35. Teuling, E., Bourgonje, A., Veenje, S., Thijssen, K., de Boer, J., van der Velde, J., Swertz, M., and Nollen, E. (2011). Modifiers of mutant huntingtin aggregation: functional conservation of C. elegans-modifiers of polyglutamine aggregation. PLoS currents *3*, RRN1255.
36. Tsuda, H., Han, S.M., Yang, Y., Tong, C., Lin, Y.Q., Mohan, K., Haueter, C., Zoghbi, A., Harati, Y., Kwan, J.*, et al.* (2008). The amyotrophic lateral sclerosis 8 protein VAPB is cleaved, secreted, and acts as a ligand for Eph receptors. Cell *133*, 963-977.
37. Tudor, E.L., Galtrey, C.M., Perkinton, M.S., Lau, K.F., De Vos, K.J., Mitchell, J.C., Ackerley, S., Hortobagyi, T., Vamos, E., Leigh, P.N.*, et al.* (2010). Amyotrophic lateral sclerosis mutant vesicle-associated membrane protein-associated protein-B transgenic mice develop TAR-DNA-binding protein-43 pathology. Neuroscience *167*, 774-785.
38. Turner, B.J., and Talbot, K. (2008). Transgenics, toxicity and therapeutics in rodent models of mutant SOD1-mediated familial ALS. Prog Neurobiol *85*, 94-134.
39. Turner, M.R., Hardiman, O., Benatar, M., Brooks, B.R., Chio, A., de Carvalho, M., Ince, P.G., Lin, C., Miller, R.G., Mitsumoto, H.*, et al.* (2013). Controversies and priorities in amyotrophic lateral sclerosis. Lancet Neurol *12*, 310-322.
40. Vaccaro, A., Tauffenberger, A., Ash, P.E., Carlomagno, Y., Petrucelli, L., and Parker, J.A. (2012). TDP-1/TDP-43 regulates stress signaling and age-dependent proteotoxicity in Caenorhabditis elegans. PLoS Genet *8*, e1002806.

41. Walker, A.K., and Atkin, J.D. (2011). Stress signaling from the endoplasmic reticulum: A central player in the pathogenesis of amyotrophic lateral sclerosis. IUBMB Life *63*, 754-763.
42. Zhang, S., Binari, R., Zhou, R., and Perrimon, N. (2010). A genomewide RNA interference screen for modifiers of aggregates formation by mutant Huntingtin in Drosophila. Genetics *184*, 1165-1179.